Three-Dimensional Kaleidoscopic Imaging - Supplemental Material

Anonymus

In this document we would like to give additional information and results that have been omitted in the paper due to space restrictions.

1. Additional Information

1.1. Infinite Number of Reflections Yields Horizon without Gaps

Due to the ray reflection law, a setup consisting of a pinhole camera and planar mirrors is equivalent to a mathematical billiard on the polygon. Mathematical billiards are objects of interest in ergodic theory. It is known here, that for every rational polygon[1] for every ray starting point and for all initial ray directions the billiard trajectory will fill all of the polygons area densily except for a countable set of directions [1]. This implies that we an observe the object everywhere in an image taken with a pinhole camera. This conclusion is true for all mirror setup where the base chamber forms a rational polygon. The same applies in the three-dimensional case. For arbitrary polygons (or polyhedrons) these facts are not yet proven but only form a hypothesis.

1.2. Number of Virtual Views

In our experiments, we found that our system generates the following number of views per reflection level:

# reflections	0	1	2	3	4	5	6	7	8	9
# views	1	3	6	12	18	14	12	12	15	15

The uneven increase can be attributed to disappearing views due to lines of discontinuity.

In Fig. 1, we show a plot of the average number of pixels per virtual view depending on the reflection level. For mostly horizontal or round objects, the plot looks similar, yielding the expected decrease in resolution for higher reflection levels. The 'Vase' data set has a different plot because it is very elongated. In the real image and for the first reflections, it is mainly seen from the top, explaining the lower number of pixels. Once the object comes into view, the graph behaves as expected.

As we can see it is not desirable to increase the number of views infinitely. In addition to the information becoming more unreliable toward the image periphery, also the number of usable pixels per view converges to zero.

2. Results on Synthetic Data

[1] i.e. a polygon with angles of the form $\frac{p}{q}\pi$, where $p,q \in \mathbb{N}$

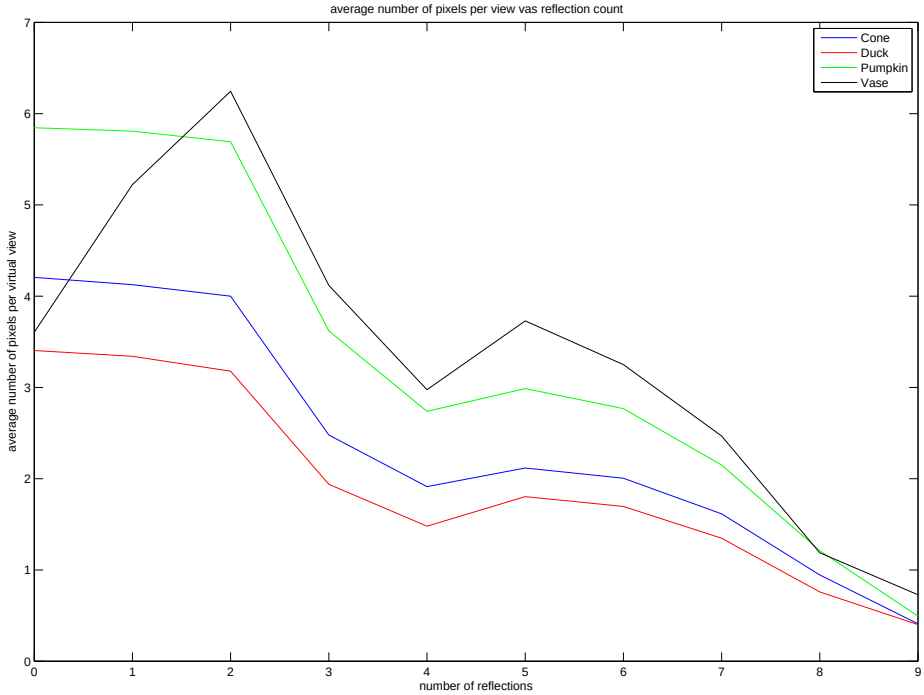

Figure 1. Average number of pixels per view per reflection level for different objects.

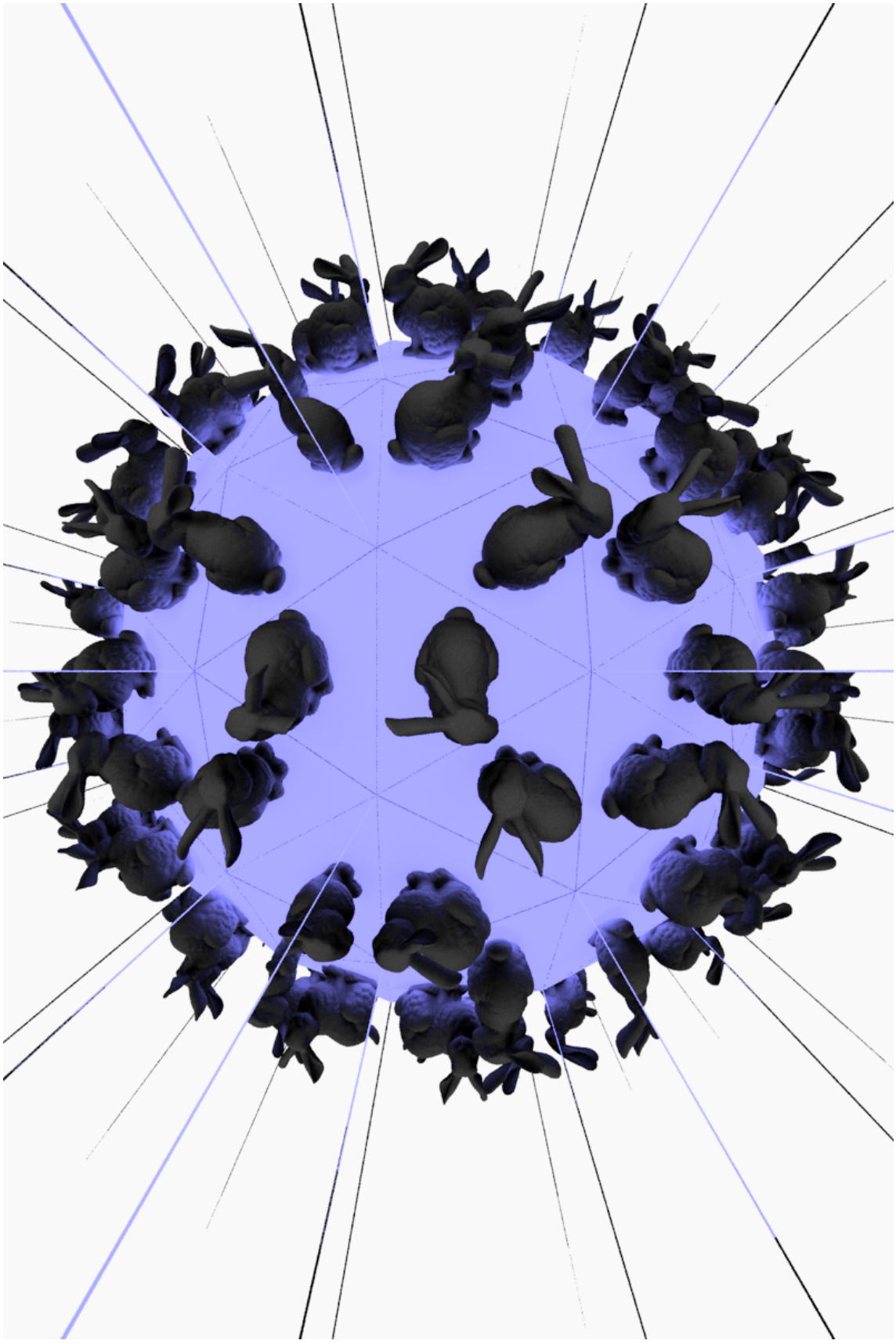

Figure 2. Bunny data set - captured image

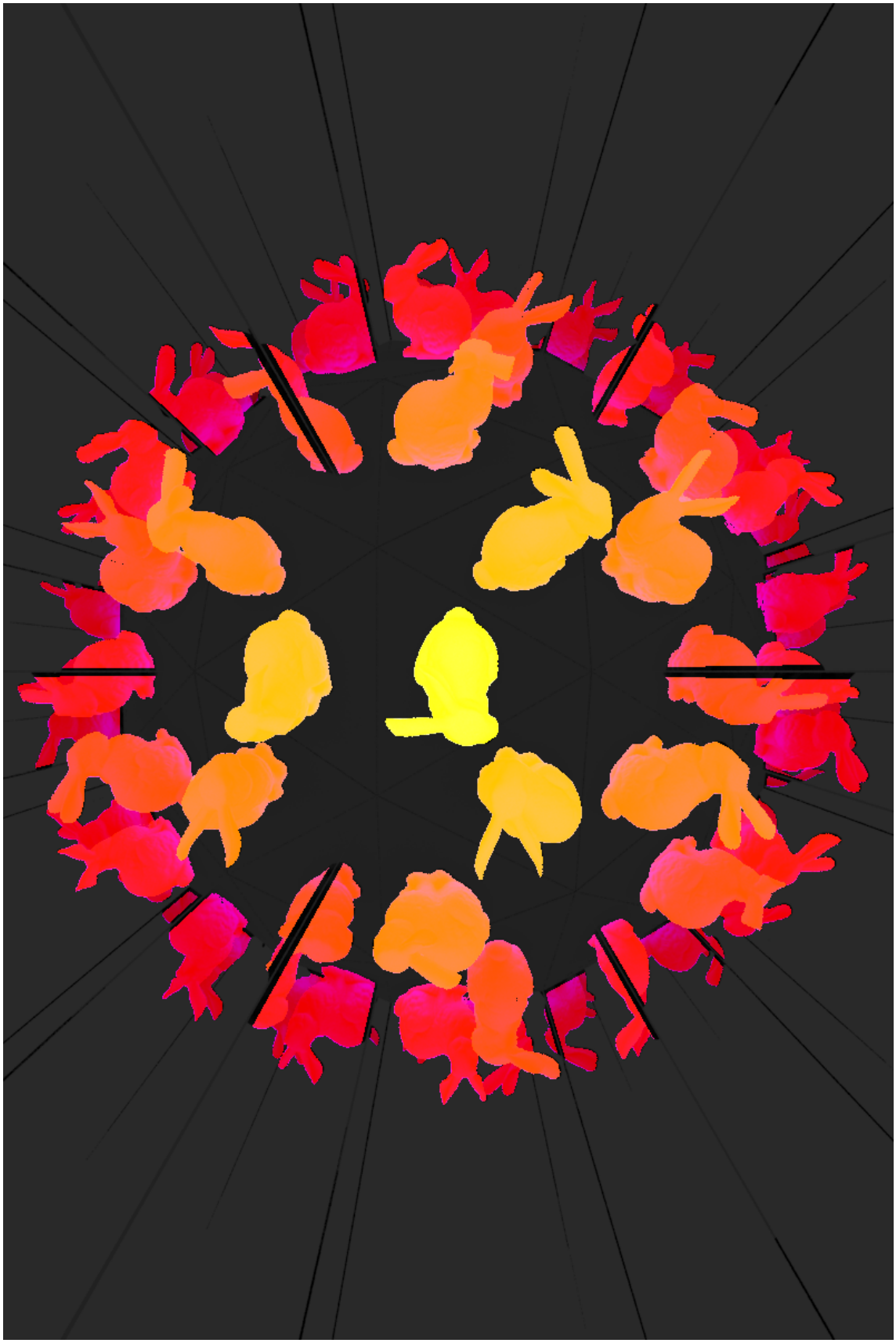

Figure 3. Bunny data set - labeled image (7 reflection levels, 9 sub-samples per pixel)

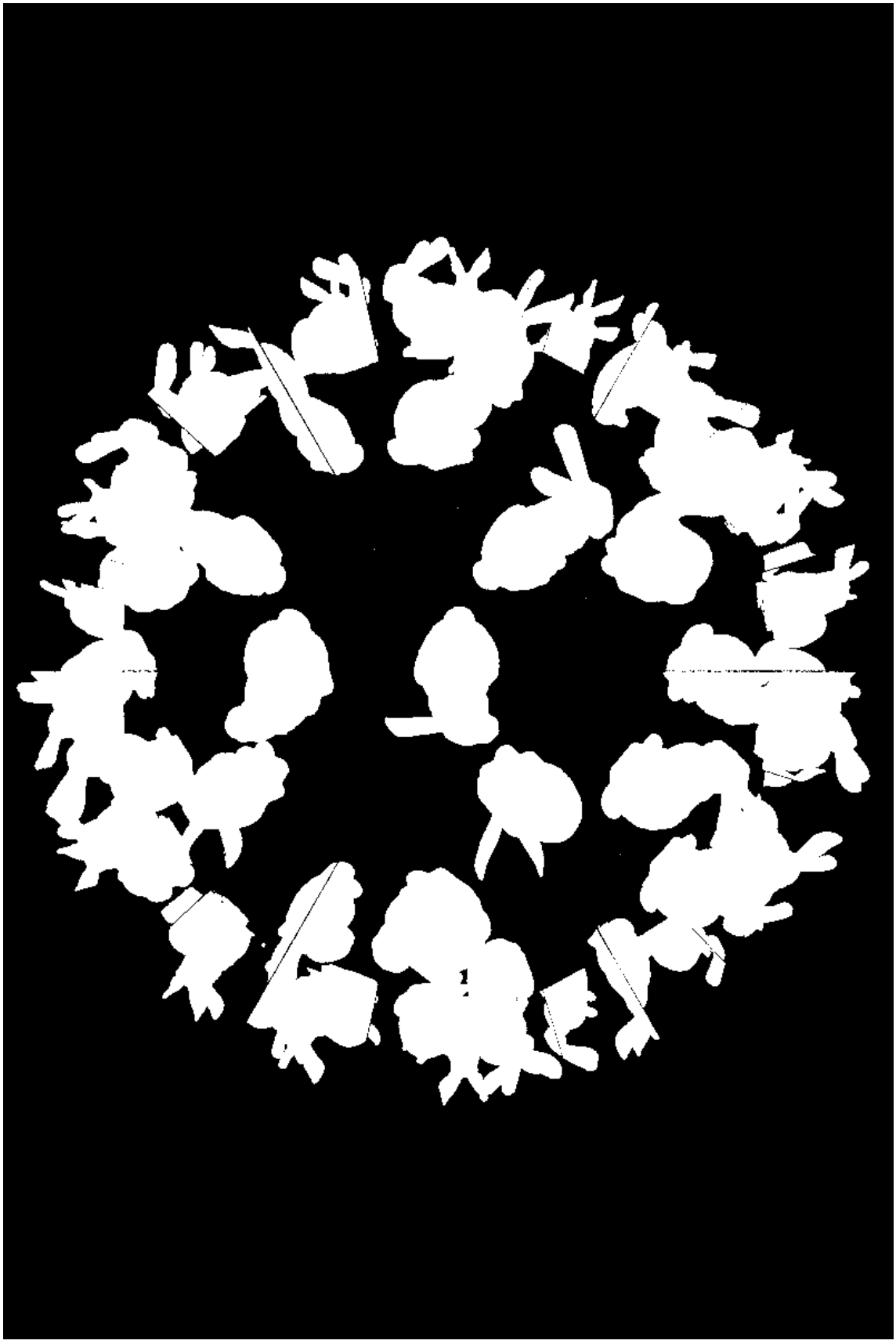

Figure 4. Bunny data set - silhouette image used to compute labeling

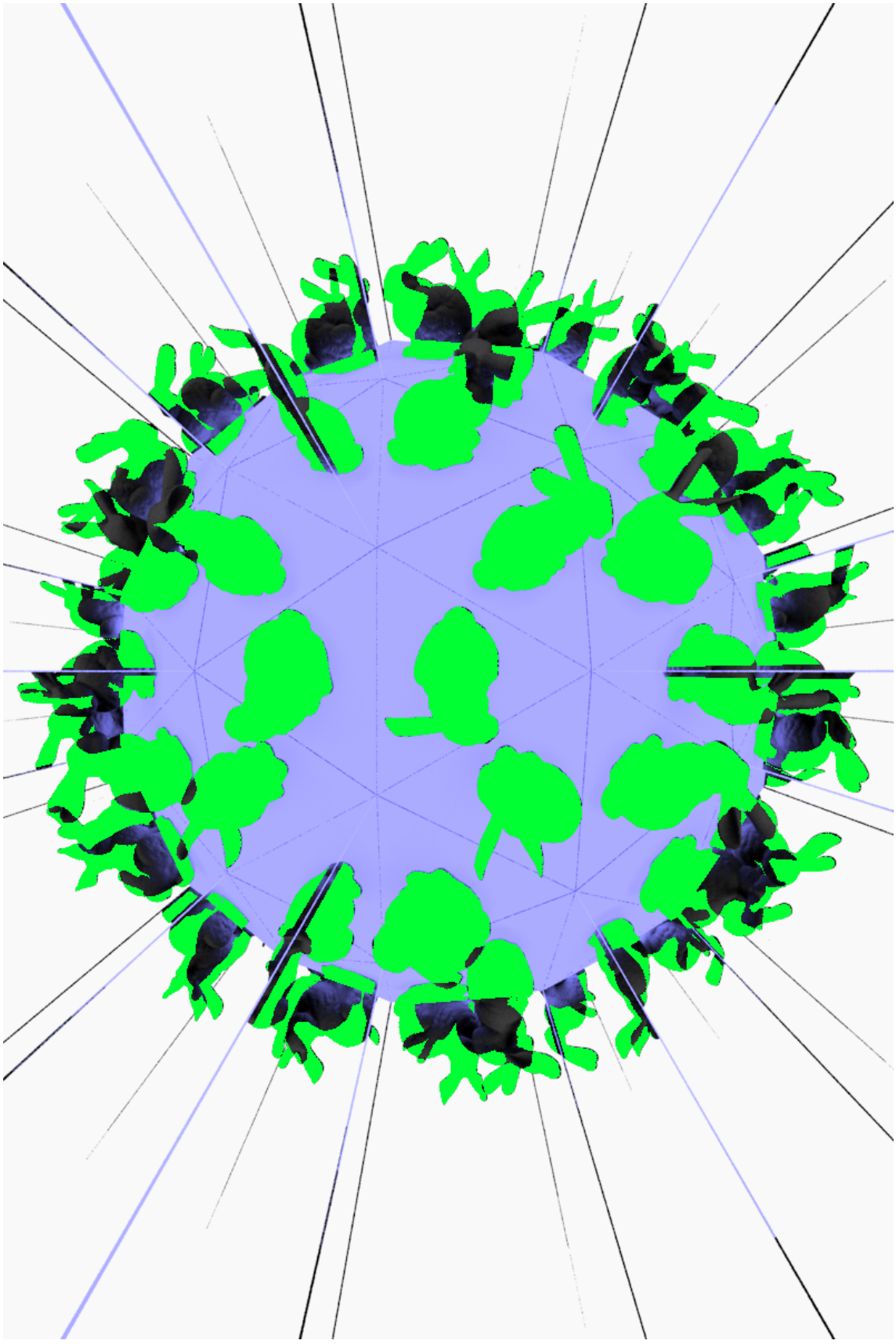

Figure 5. Bunny data set - reliable pixels

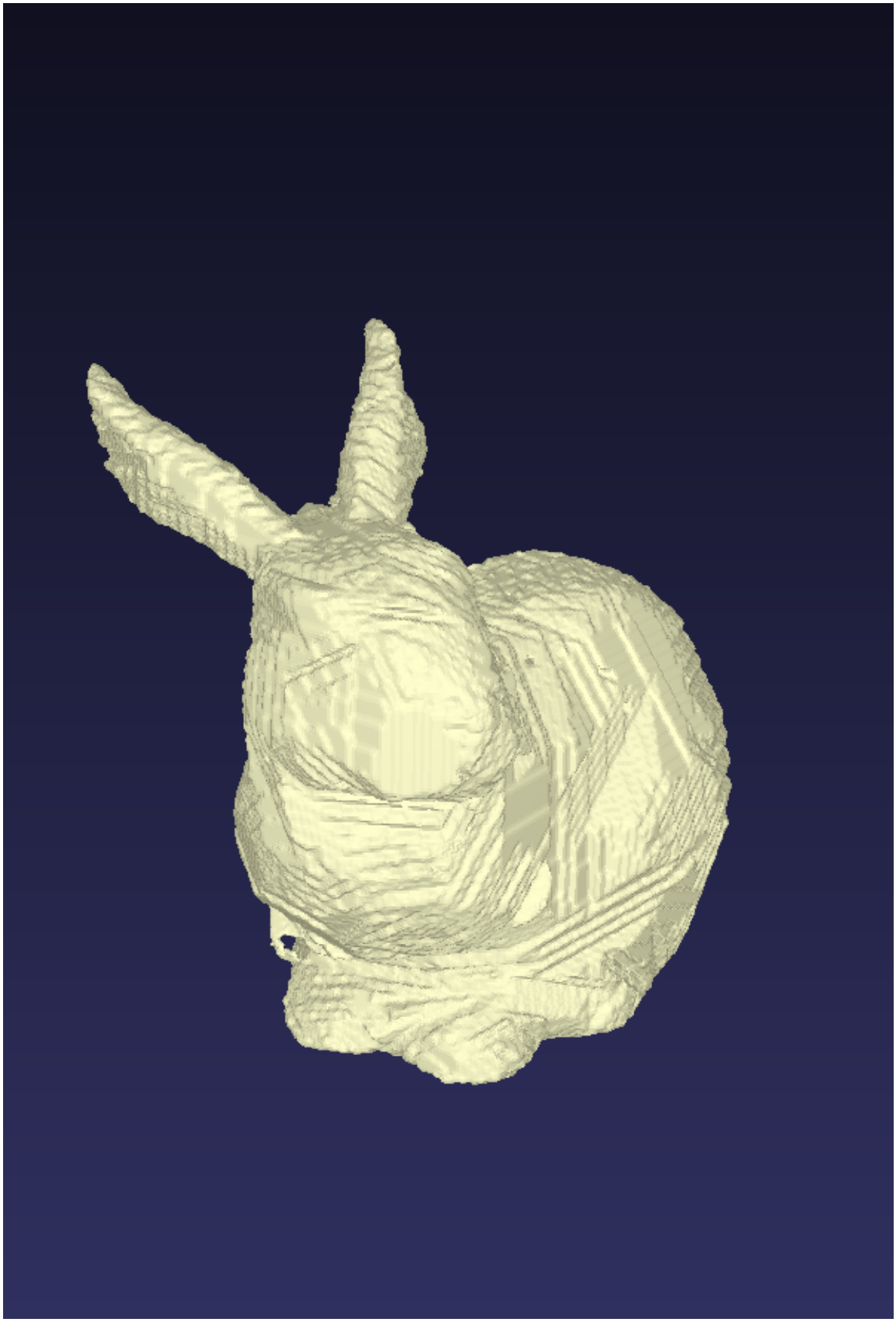

Figure 6. Bunny data set - visual hull $256 \times 332 \times 256$

3. Results on Real Data

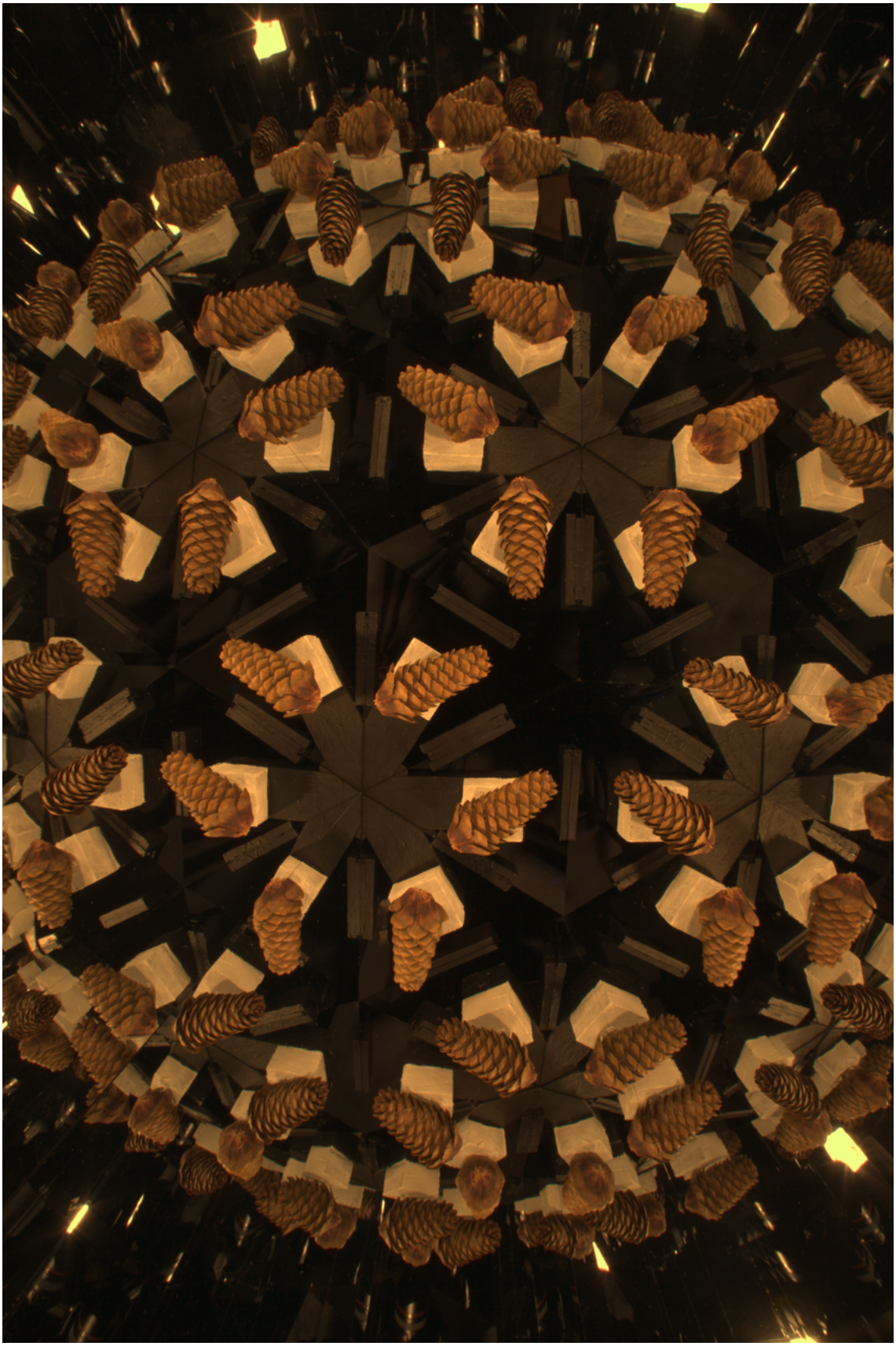

Figure 7. Cone1 data set - captured image

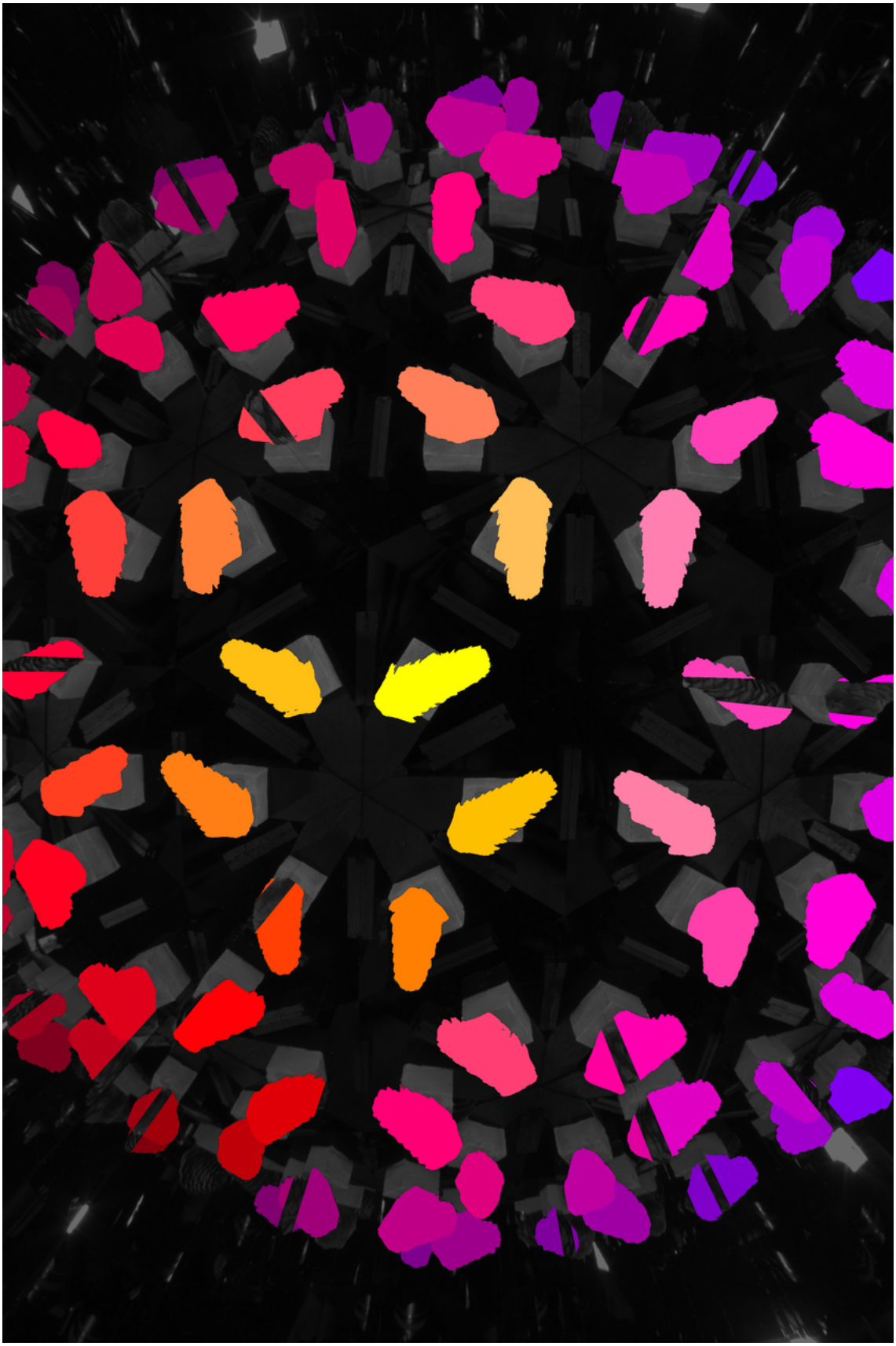

Figure 8. Cone data set - labeled image (8 reflection levels, 9 sub-samples per pixel)

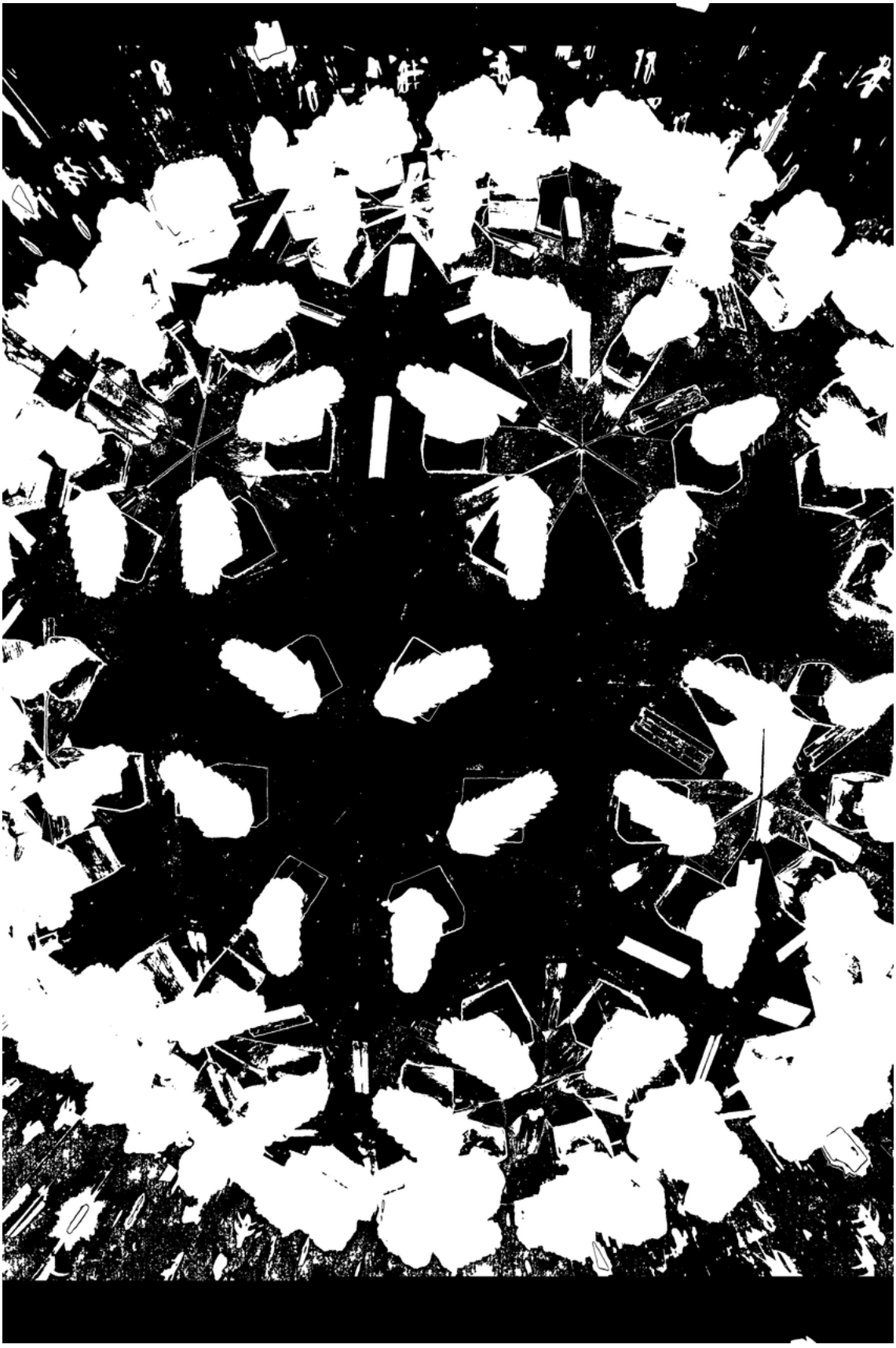

Figure 9. Cone data set - silhouette image used to compute labeling

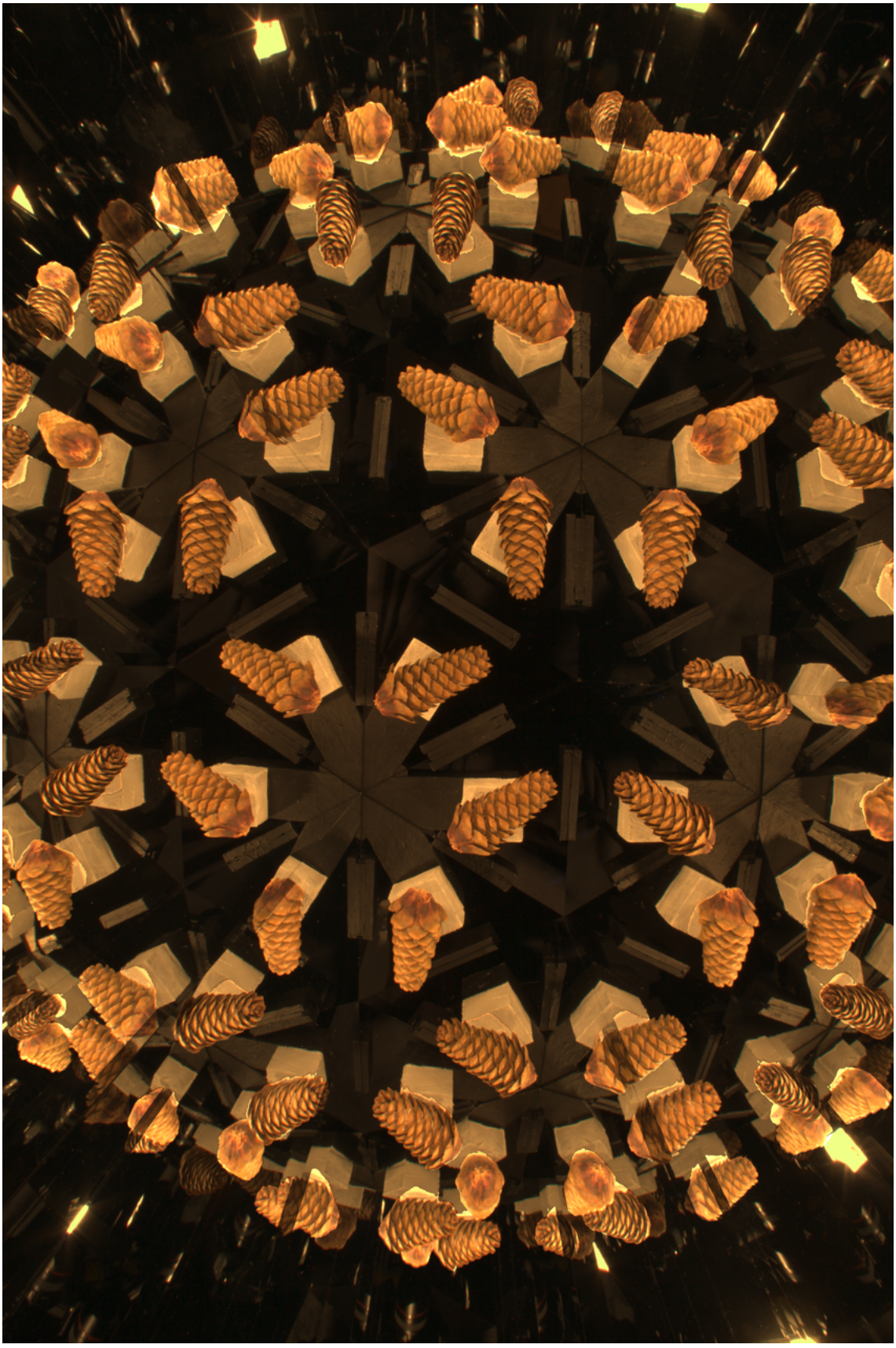

Figure 10. Cone data set - radiometrically compensated imaged

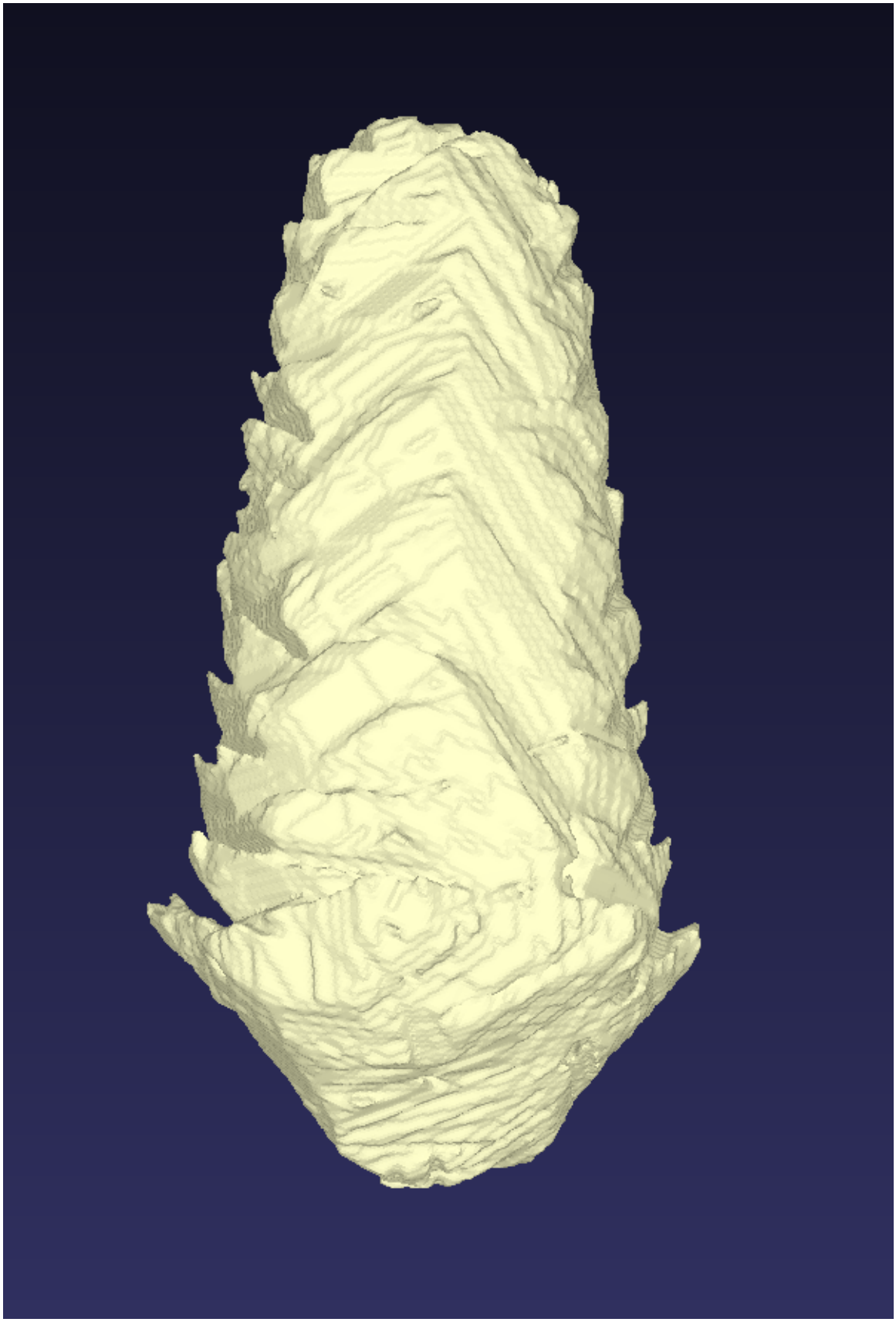

Figure 11. Cone data set - visual hull $256 \times 256 \times 236$

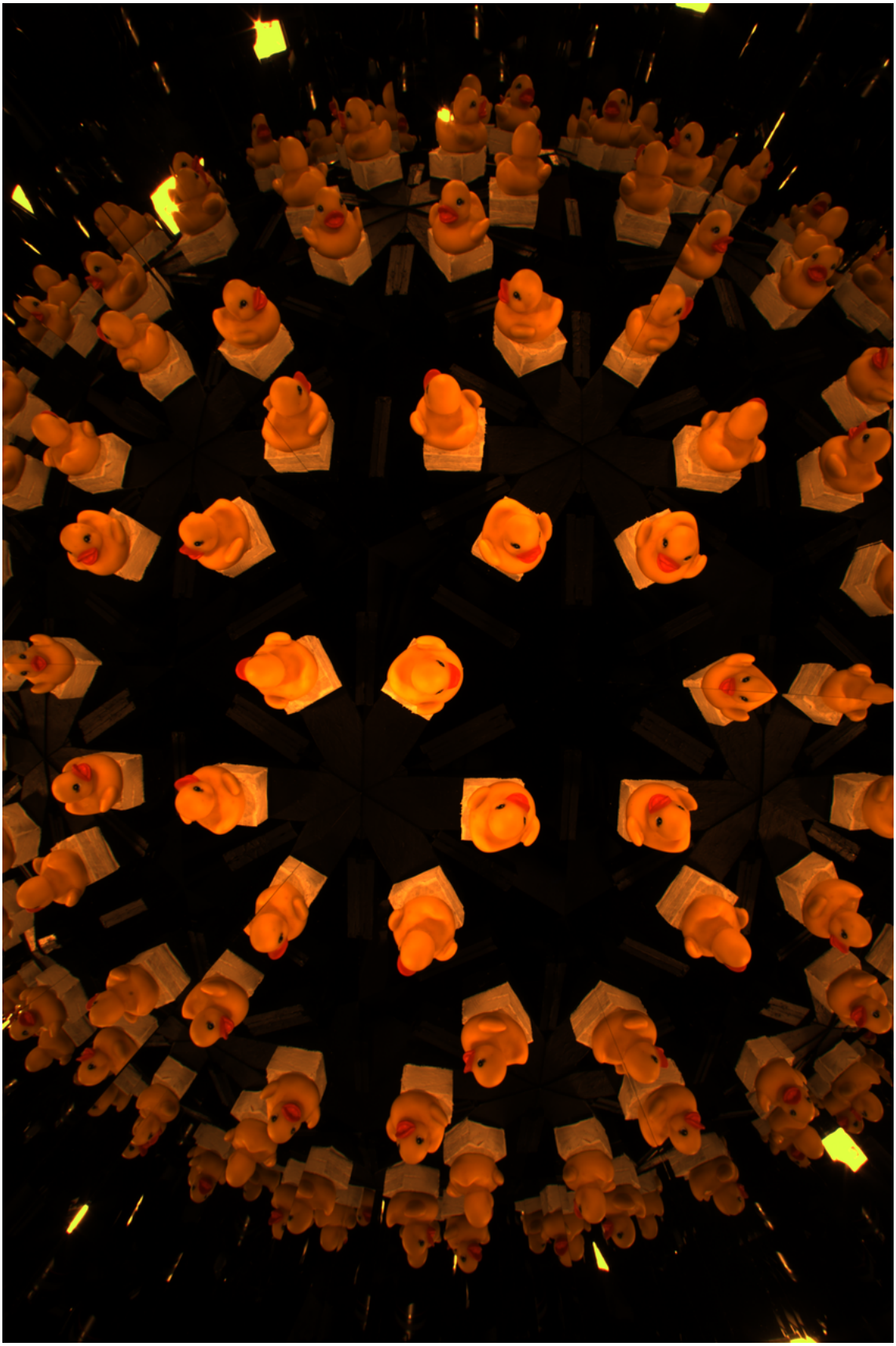

Figure 12. Duck data set - captured image

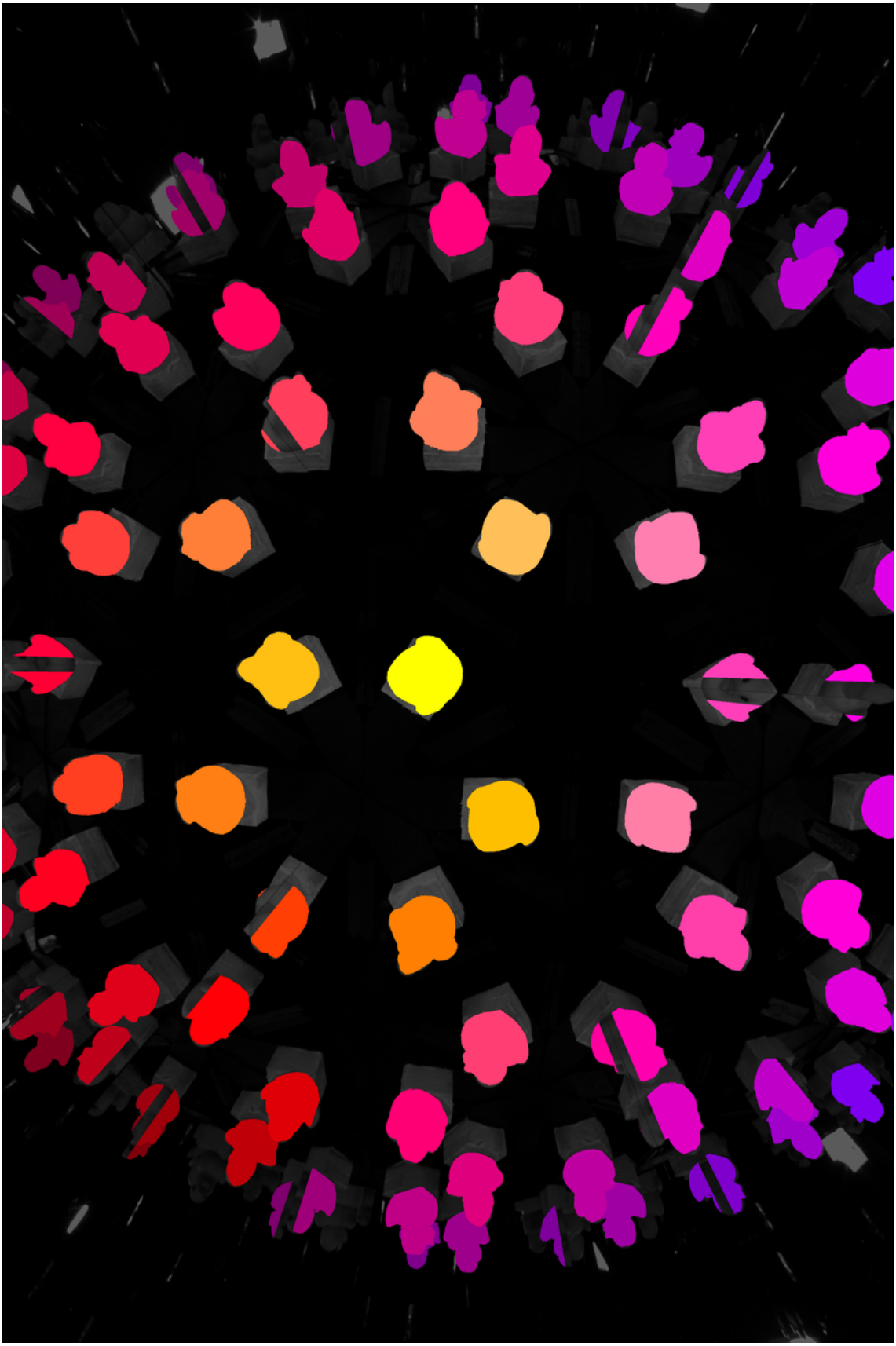

Figure 13. Duck data set - labeled image (8 reflection levels, 9 sub-samples per pixel)

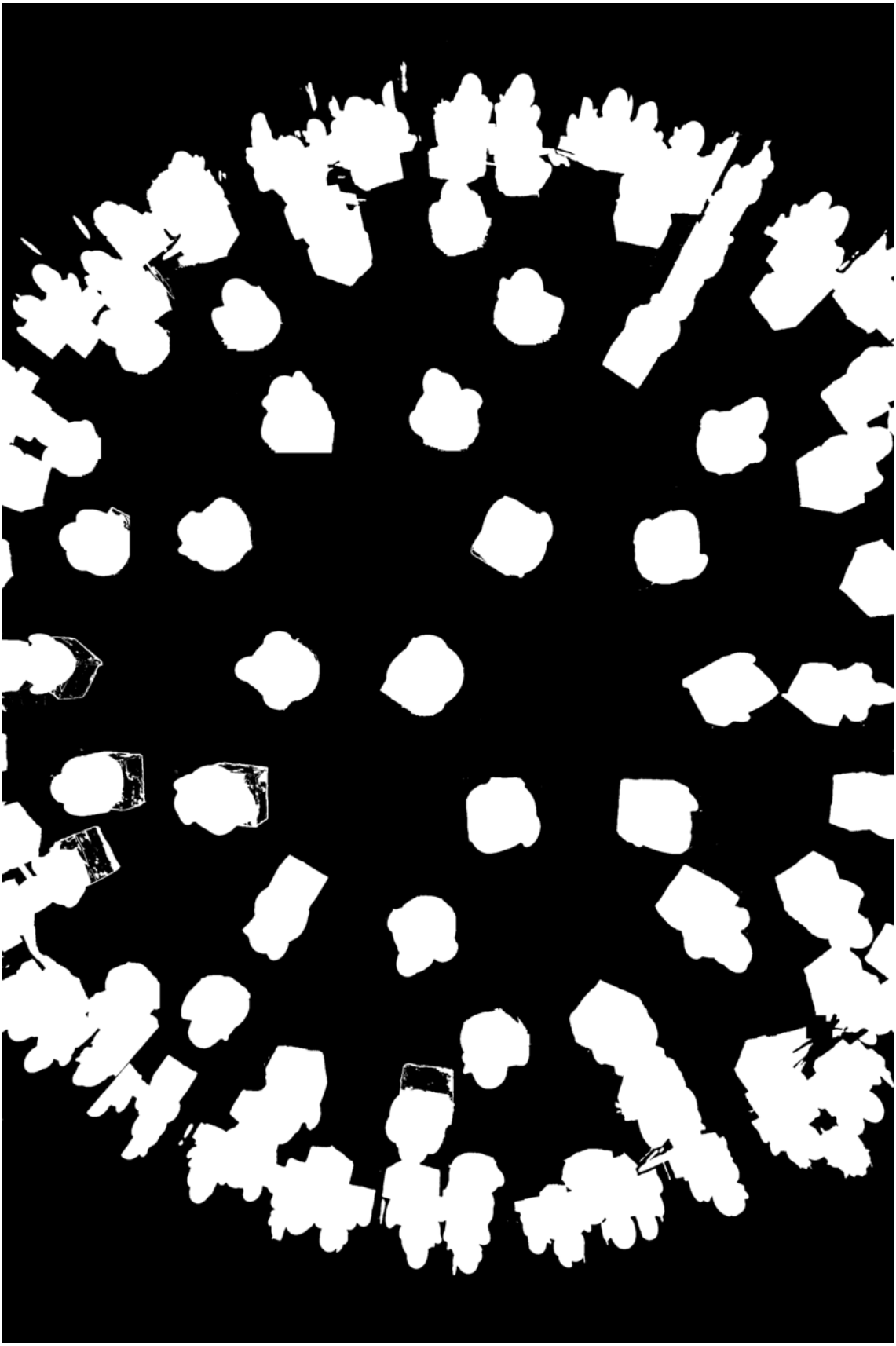

Figure 14. Duck data set - silhouette image used to compute labeling

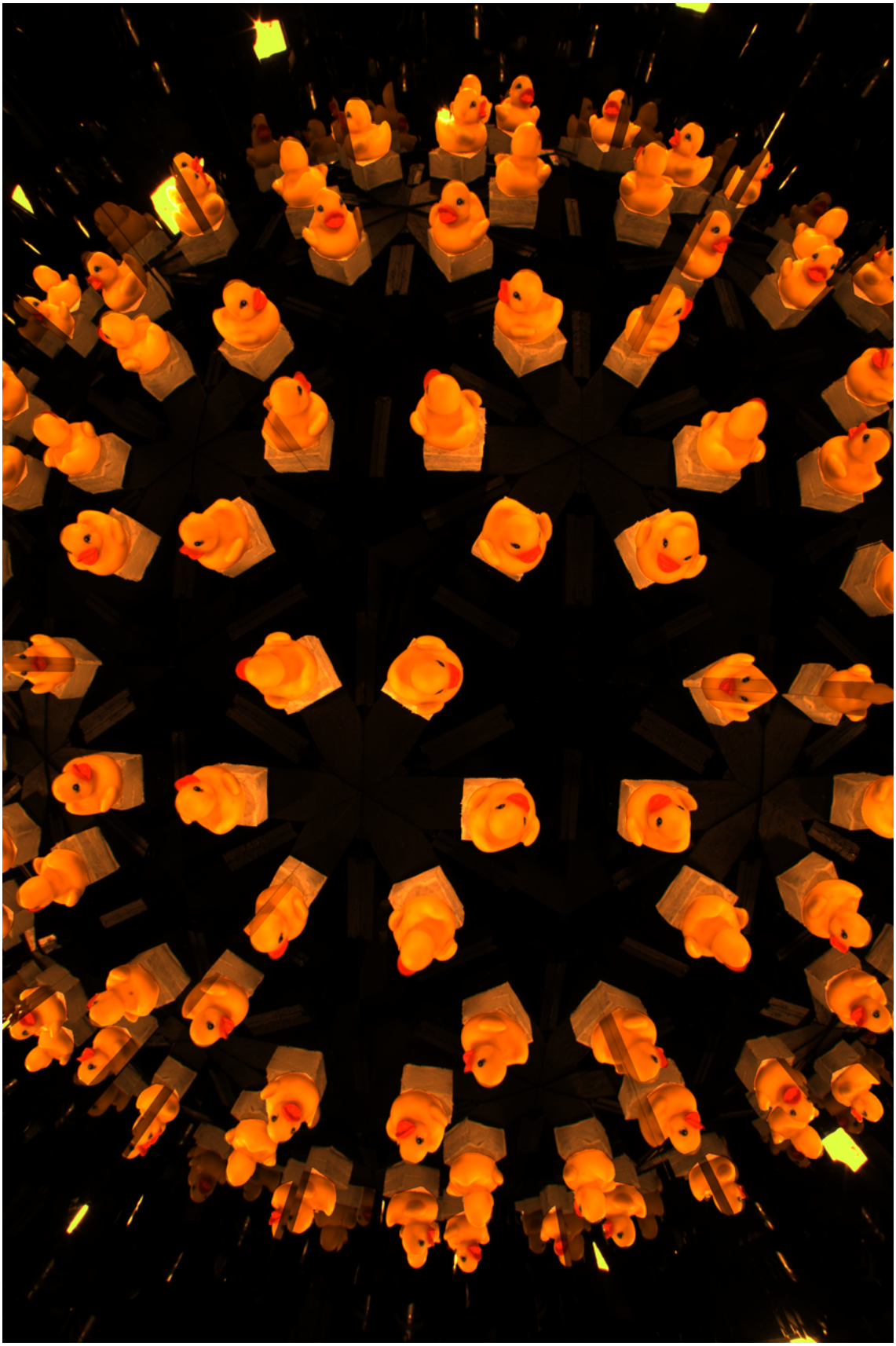

Figure 15. Duck data set - radiometrically compensated imaged

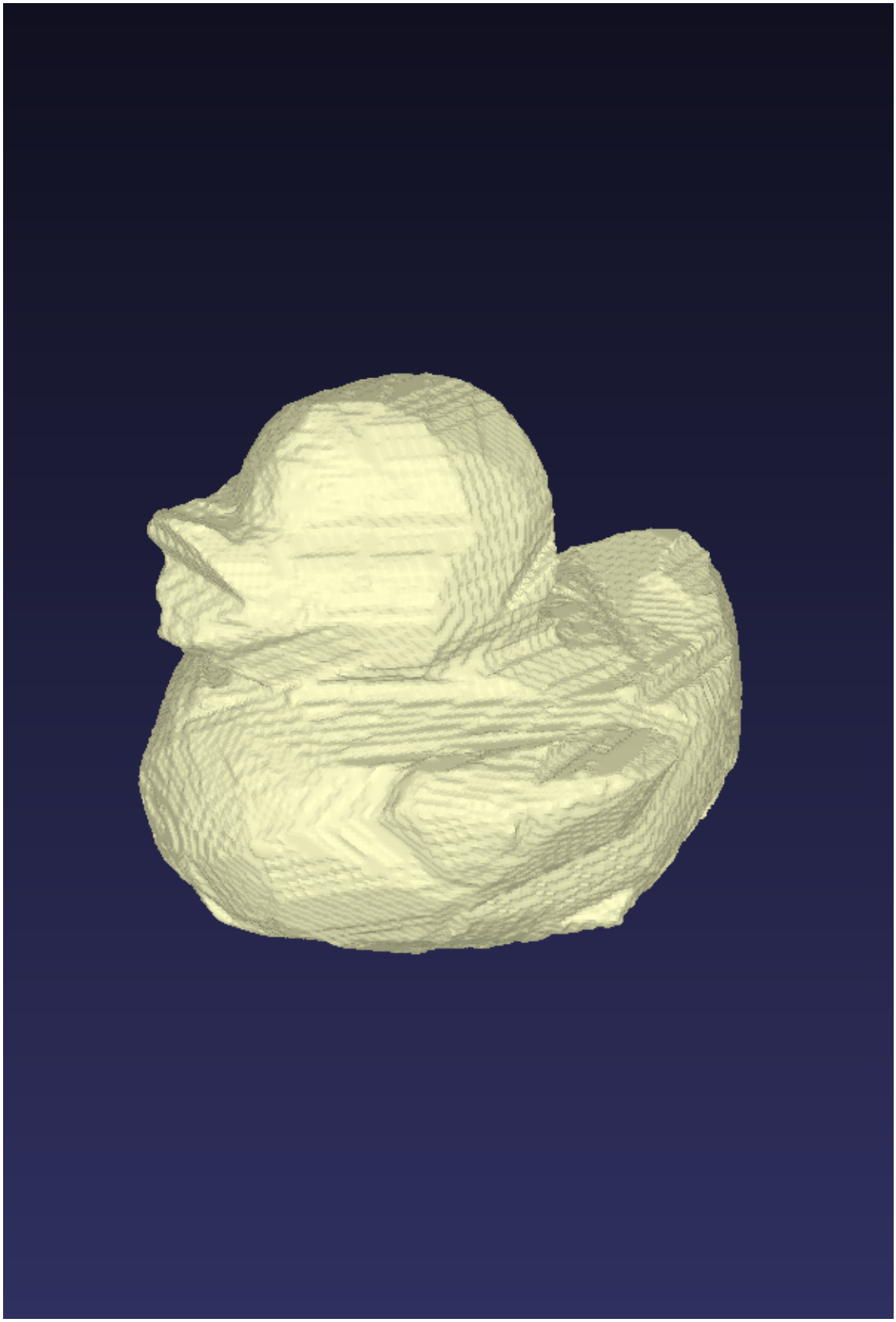

Figure 16. Duck data set - visual hull $256 \times 256 \times 221$

Figure 17. Pumpkin data set - captured image

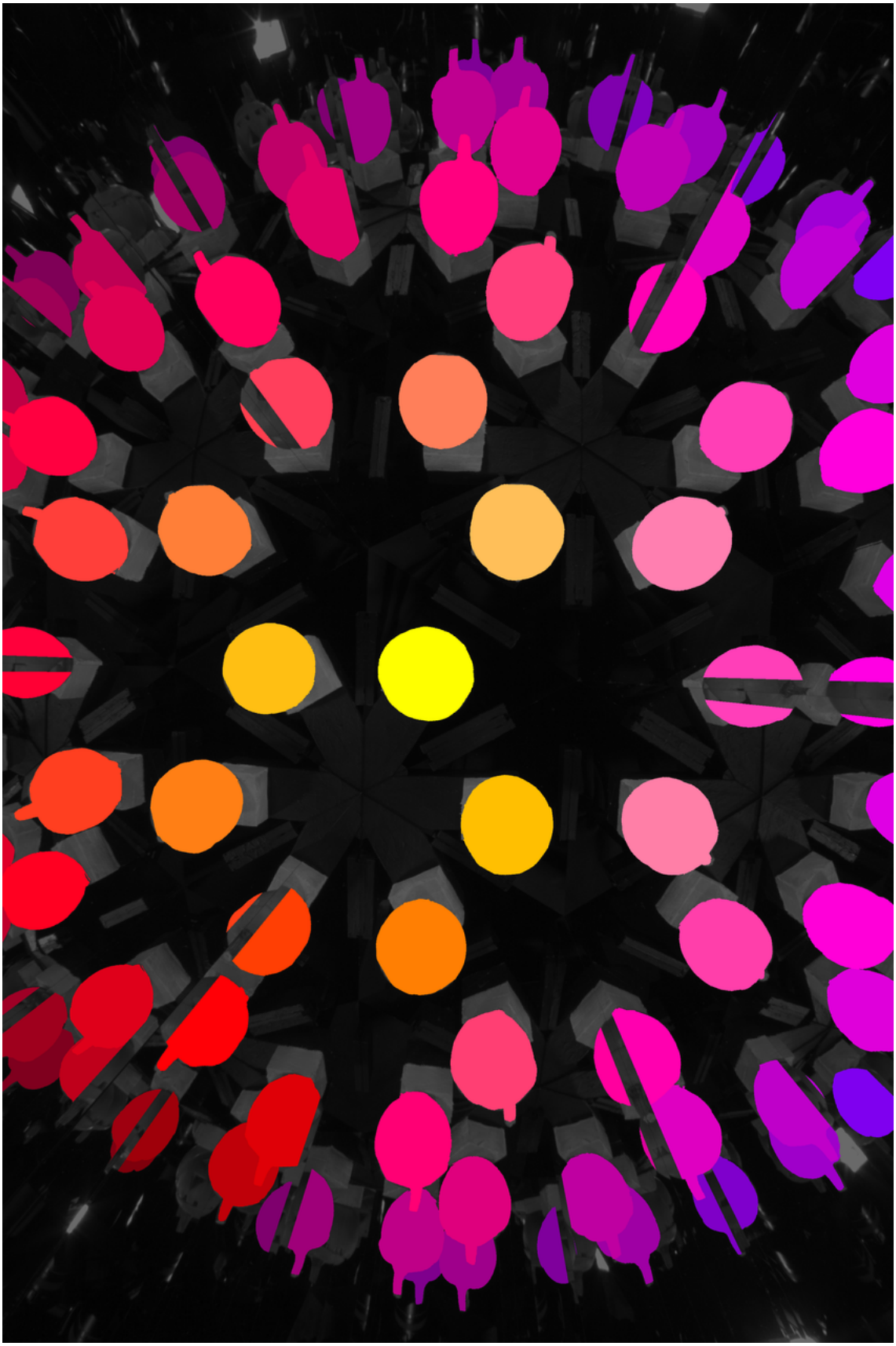

Figure 18. Pumpkin data set - labeled image (8 reflection levels, 9 sub-samples per pixel)

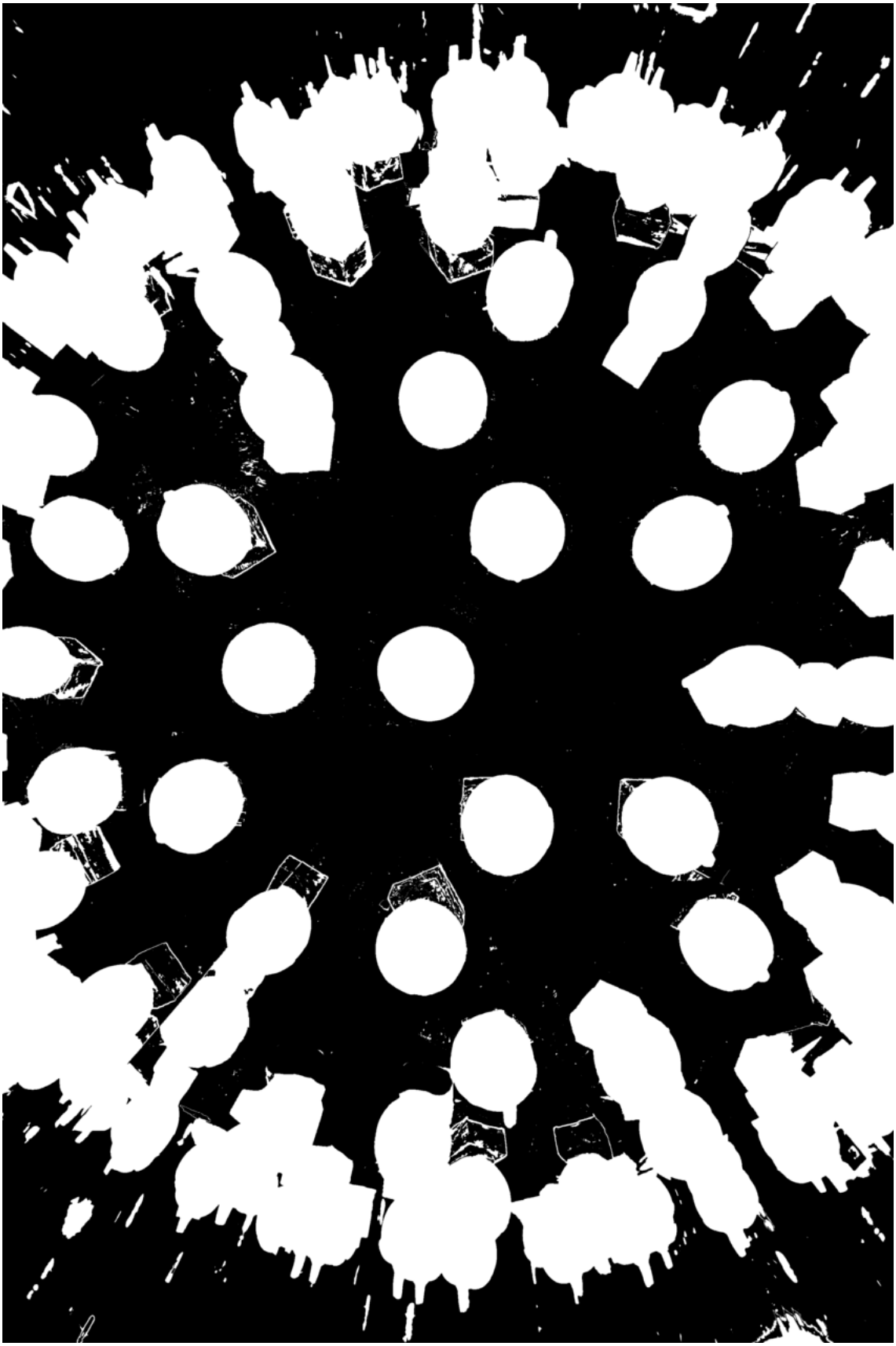

Figure 19. Pumpkin data set - silhouette image used to compute labeling

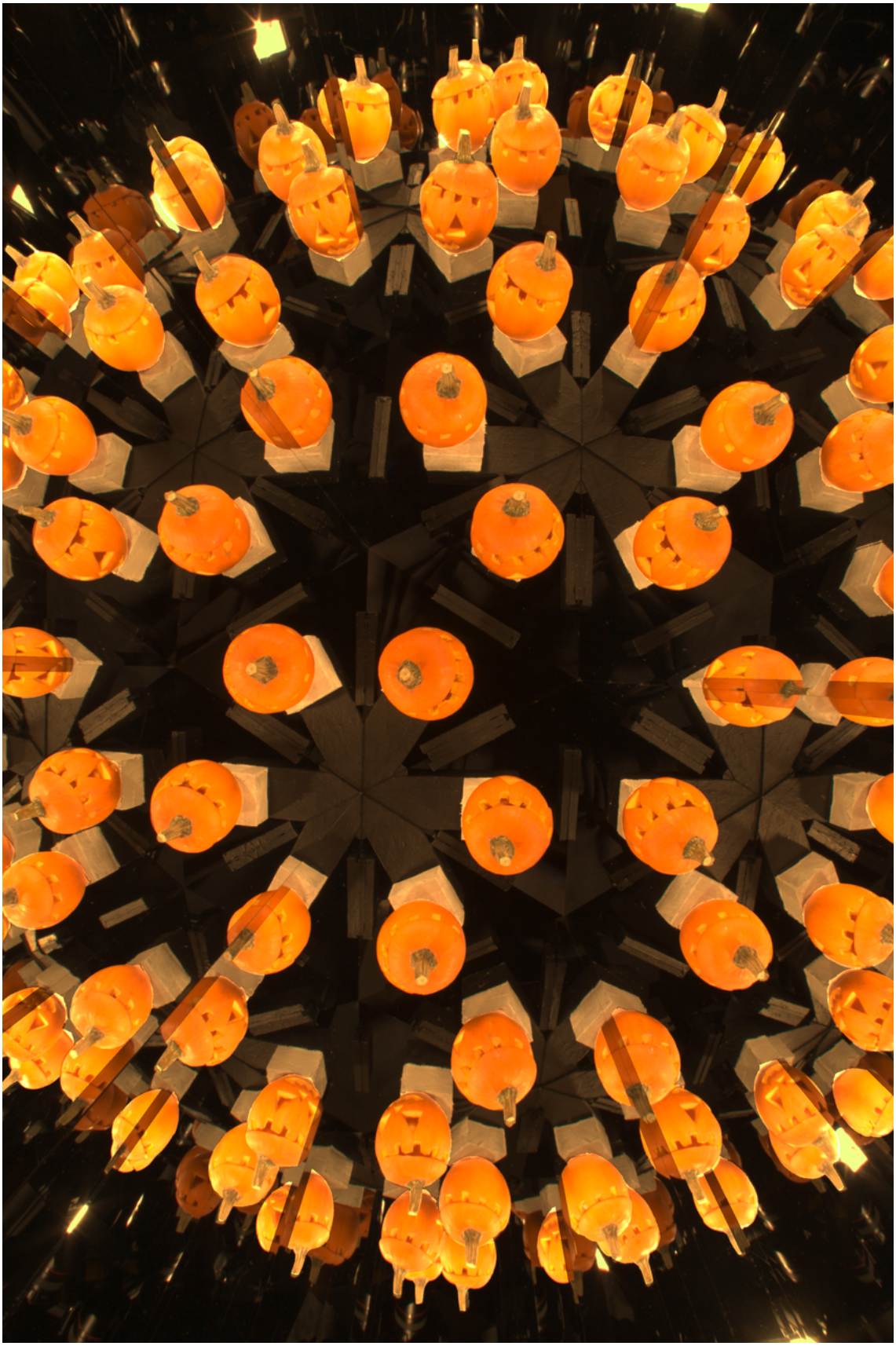

Figure 20. Pumpkin data set - radiometrically compensated imaged

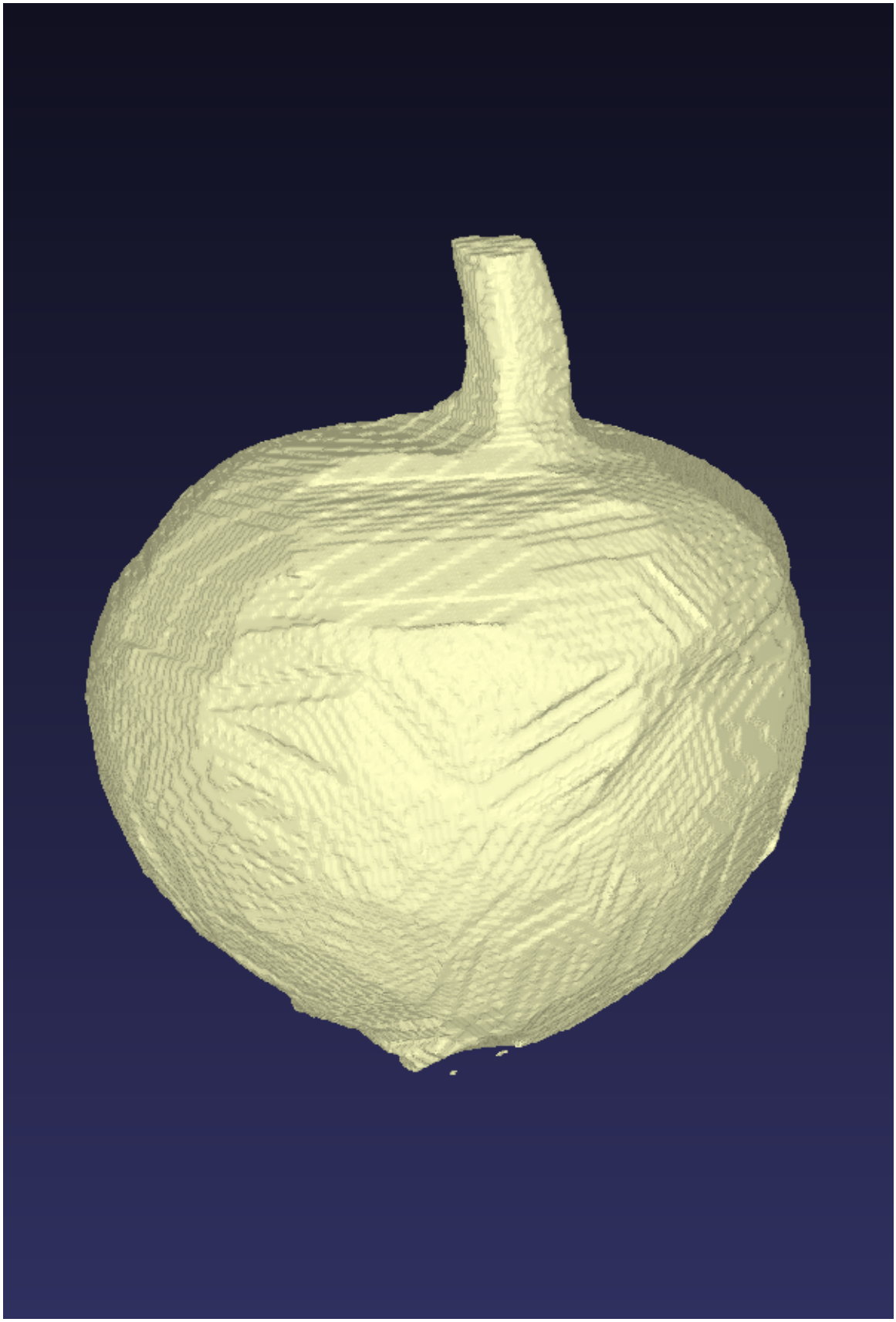

Figure 21. Pumpkin data set - visual hull $300 \times 300 \times 346$

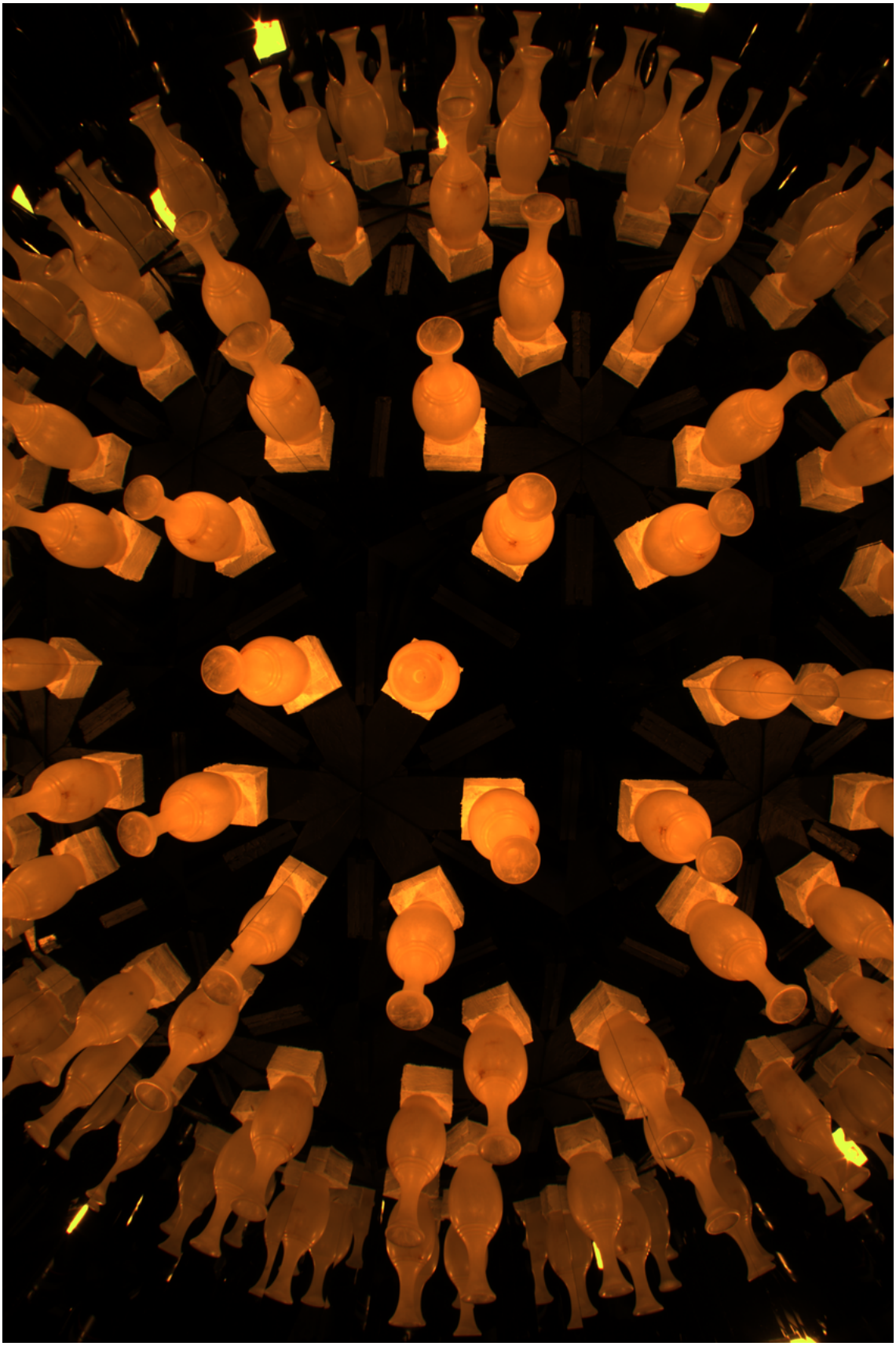

Figure 22. Vase data set - captured image

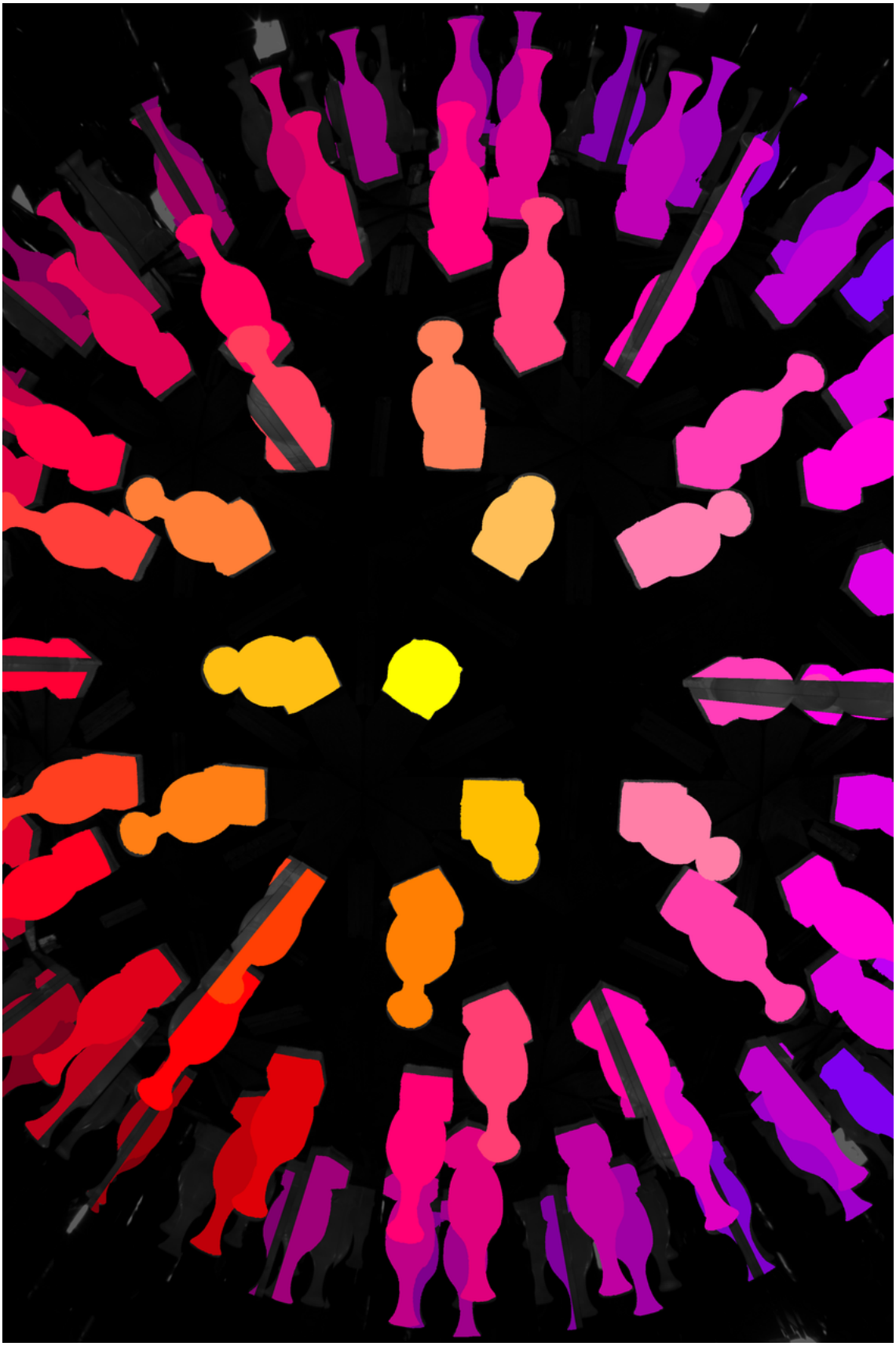

Figure 23. Vase data set - labeled image (8 reflection levels, 9 sub-samples per pixel)

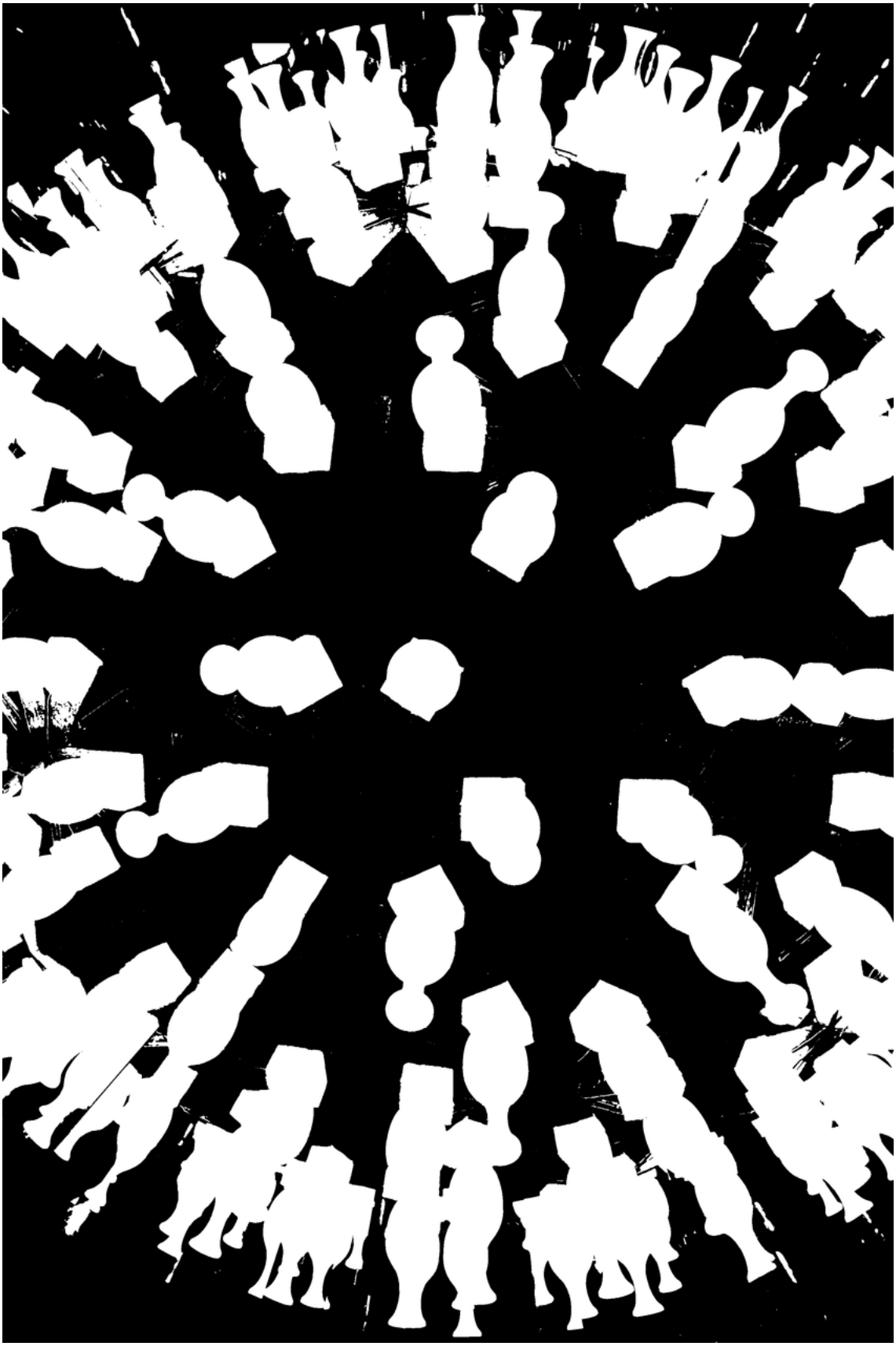

Figure 24. Vase data set - silhouette image used to compute labeling

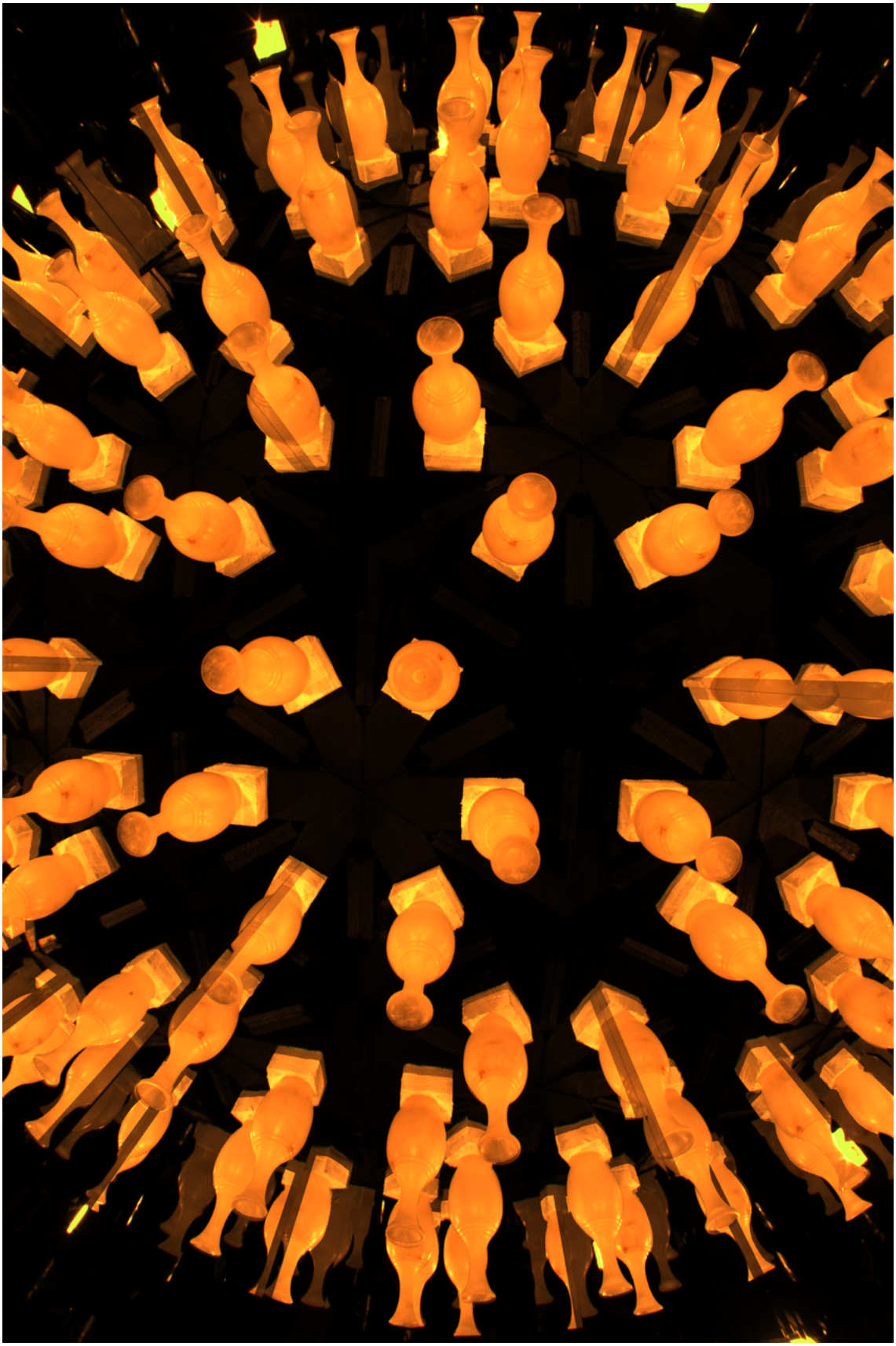

Figure 25. Vase data set - radiometrically compensated imaged

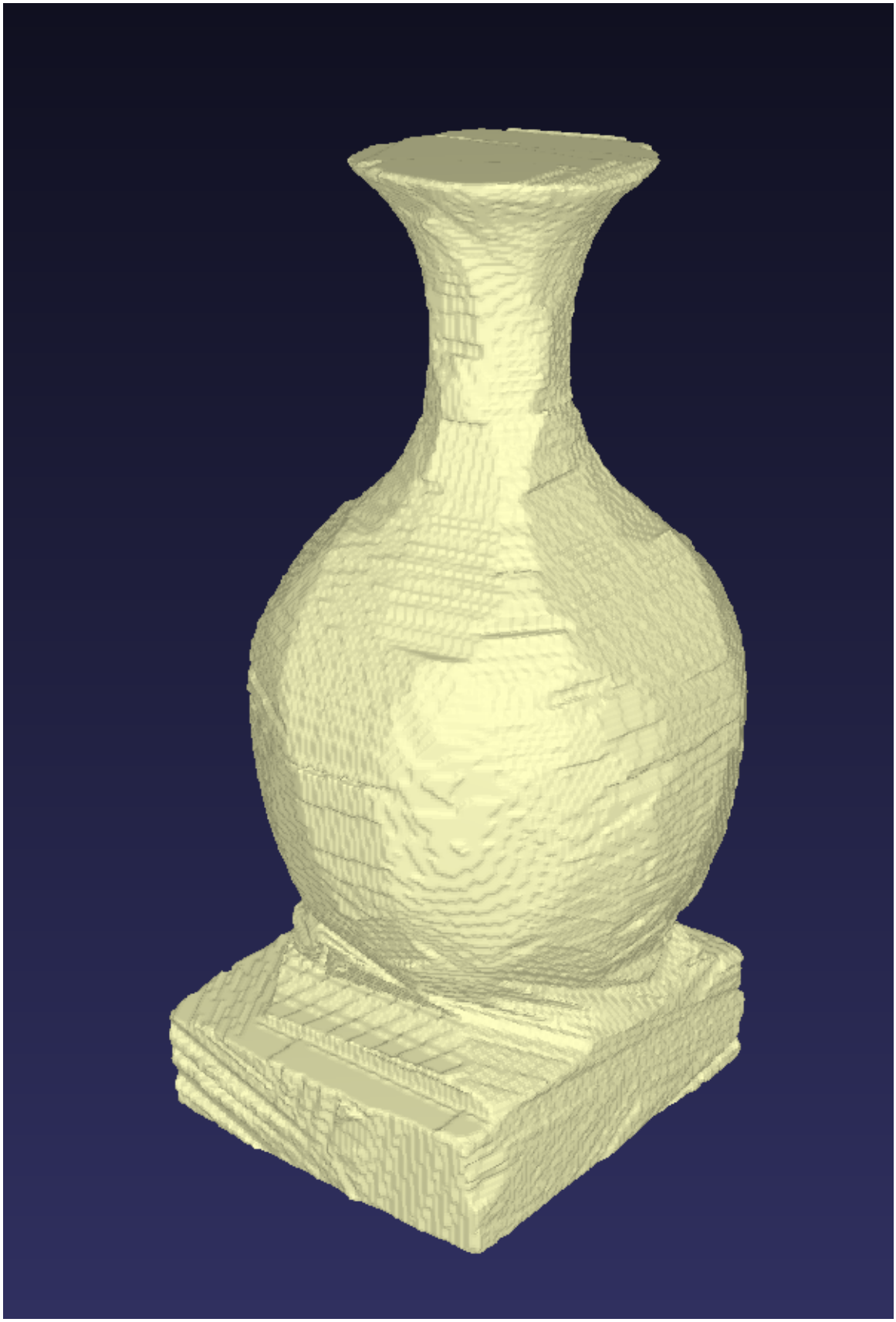

Figure 26. Vase data set - visual hull $256 \times 256 \times 354$

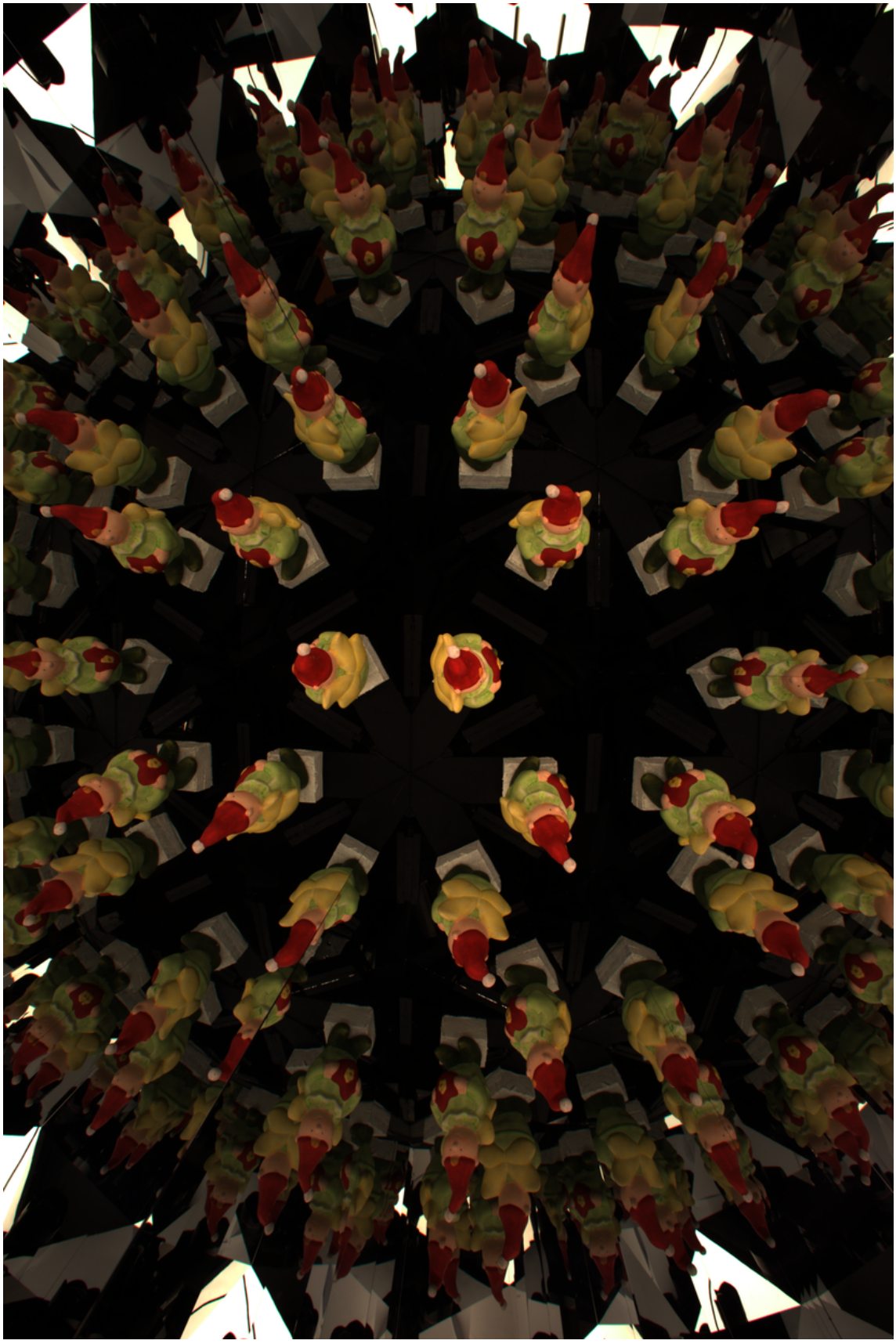

Figure 27. Prince data set - captured image

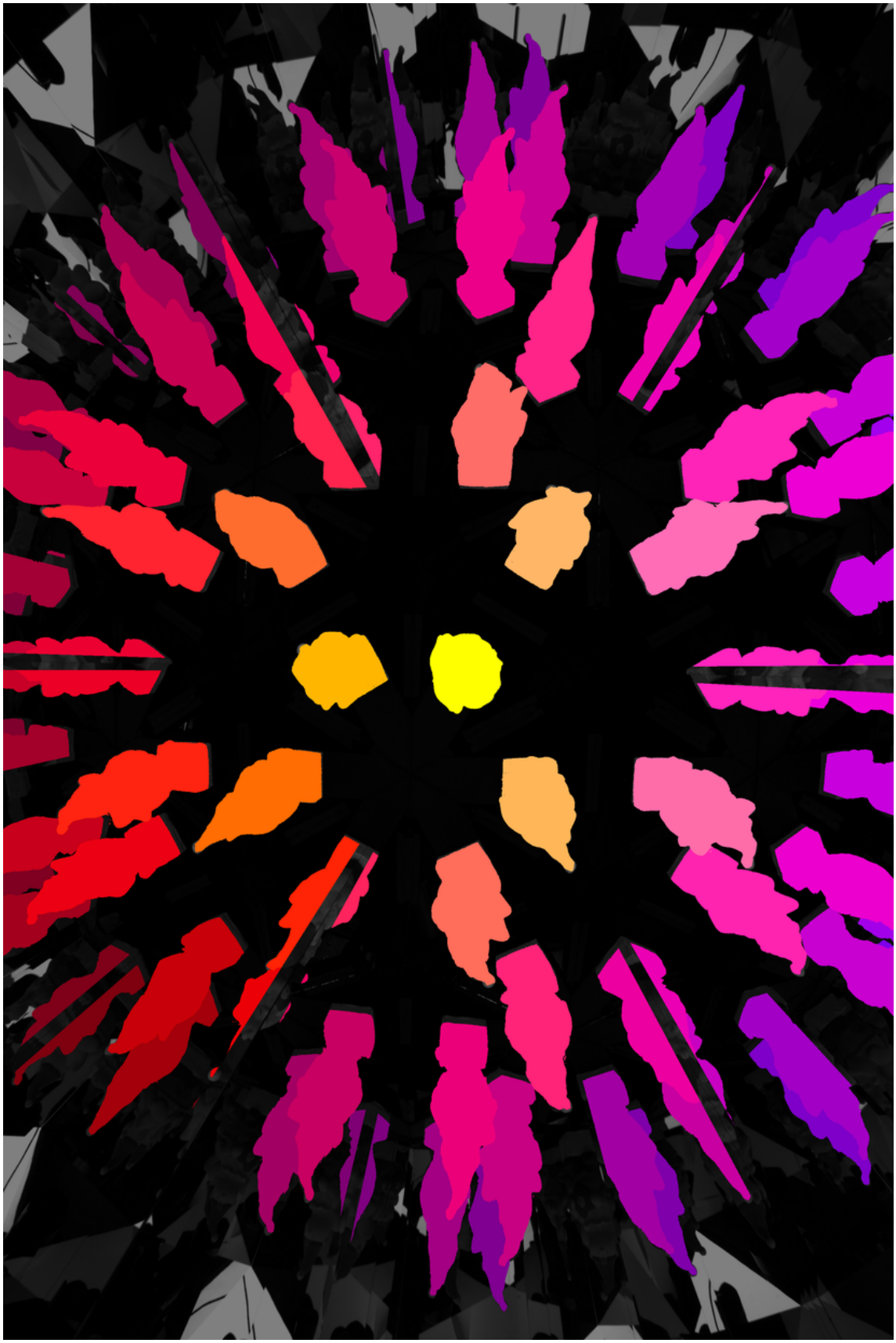

Figure 28. Prince data set - labeled image (7 reflection levels, 9 sub-samples per pixel)

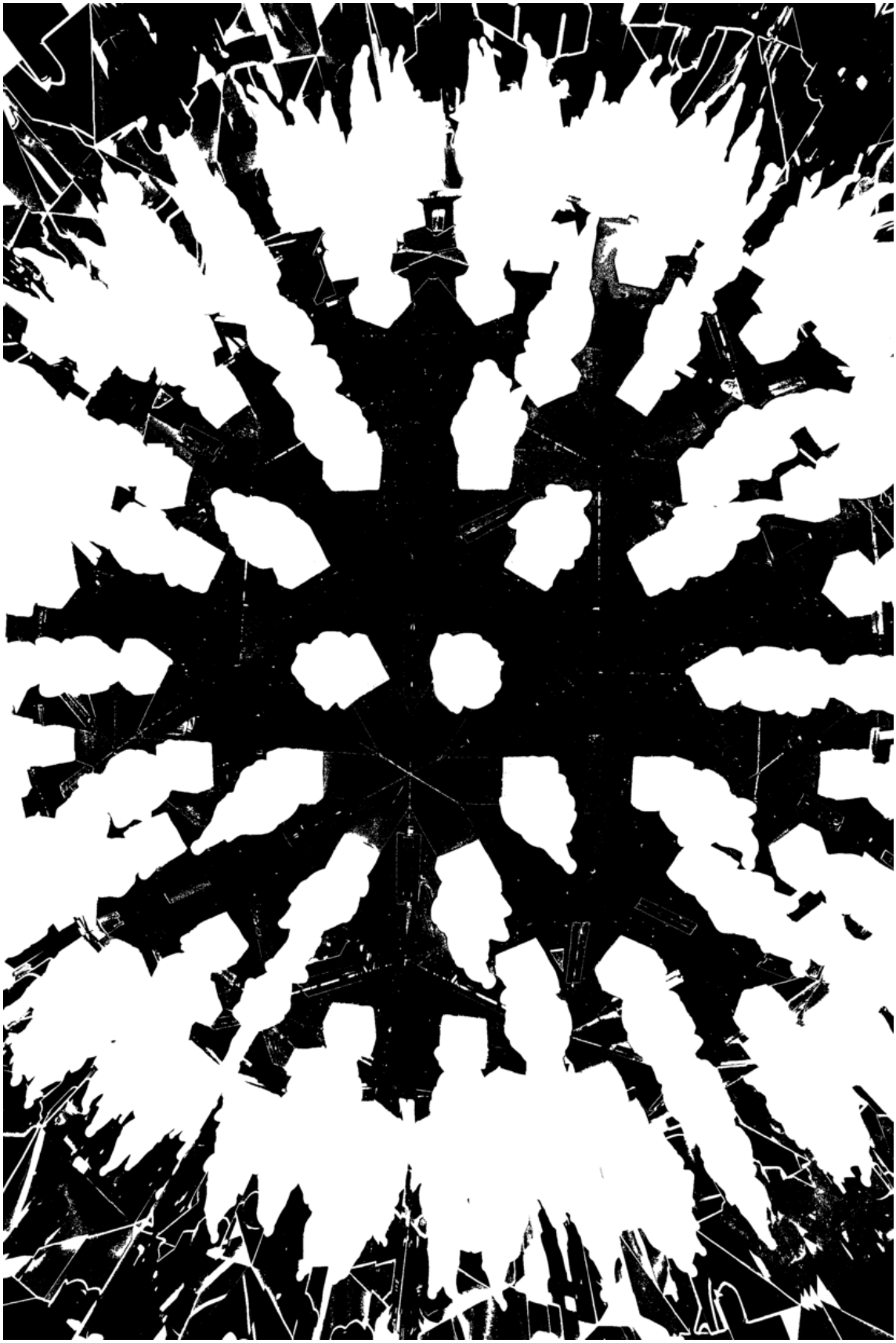

Figure 29. Prince data set - silhouette image used to compute labeling

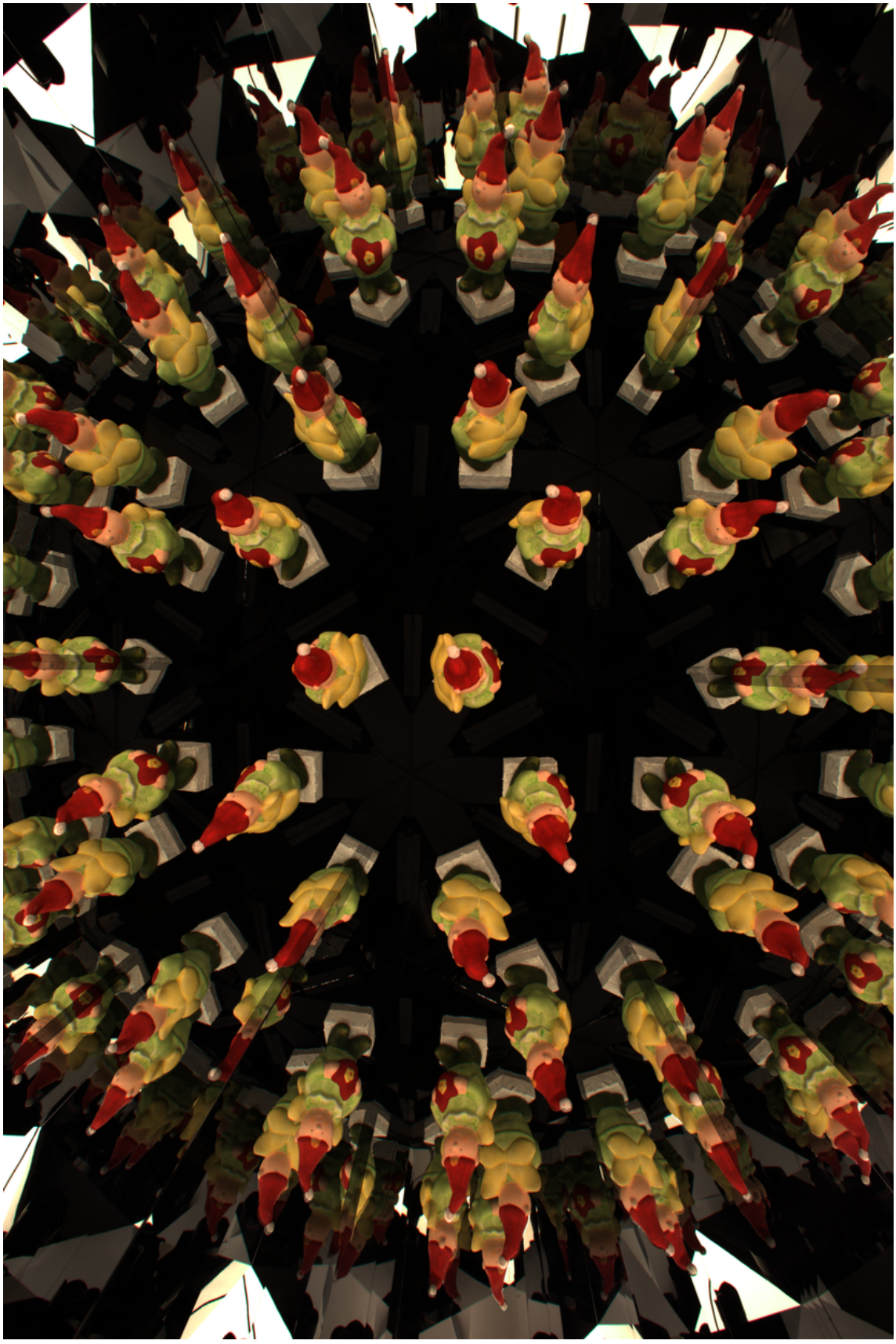

Figure 30. Prince data set - radiometrically compensated imaged

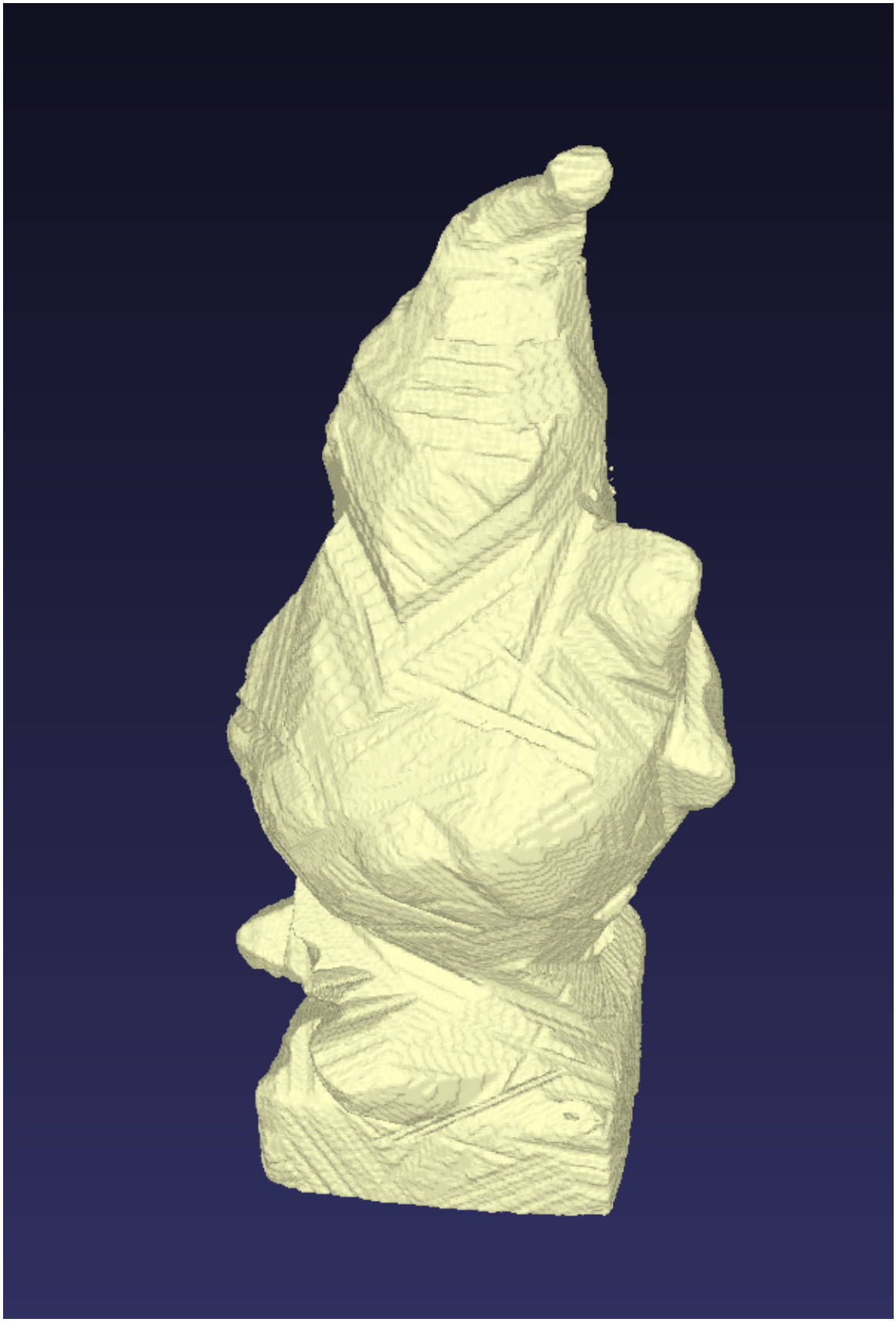

Figure 31. Prince data set - visual hull $256 \times 256 \times 354$

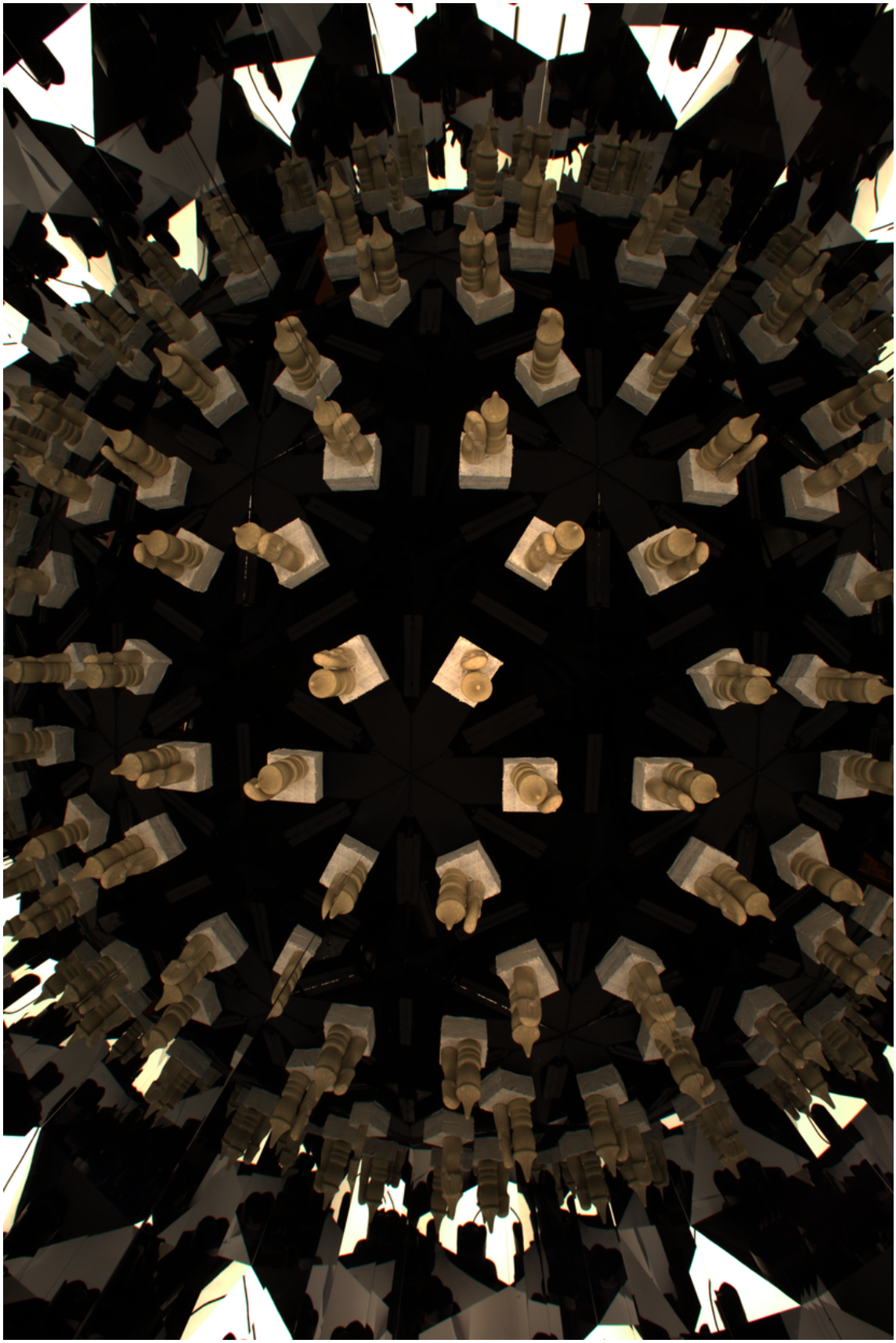

Figure 32. Chess data set - captured image

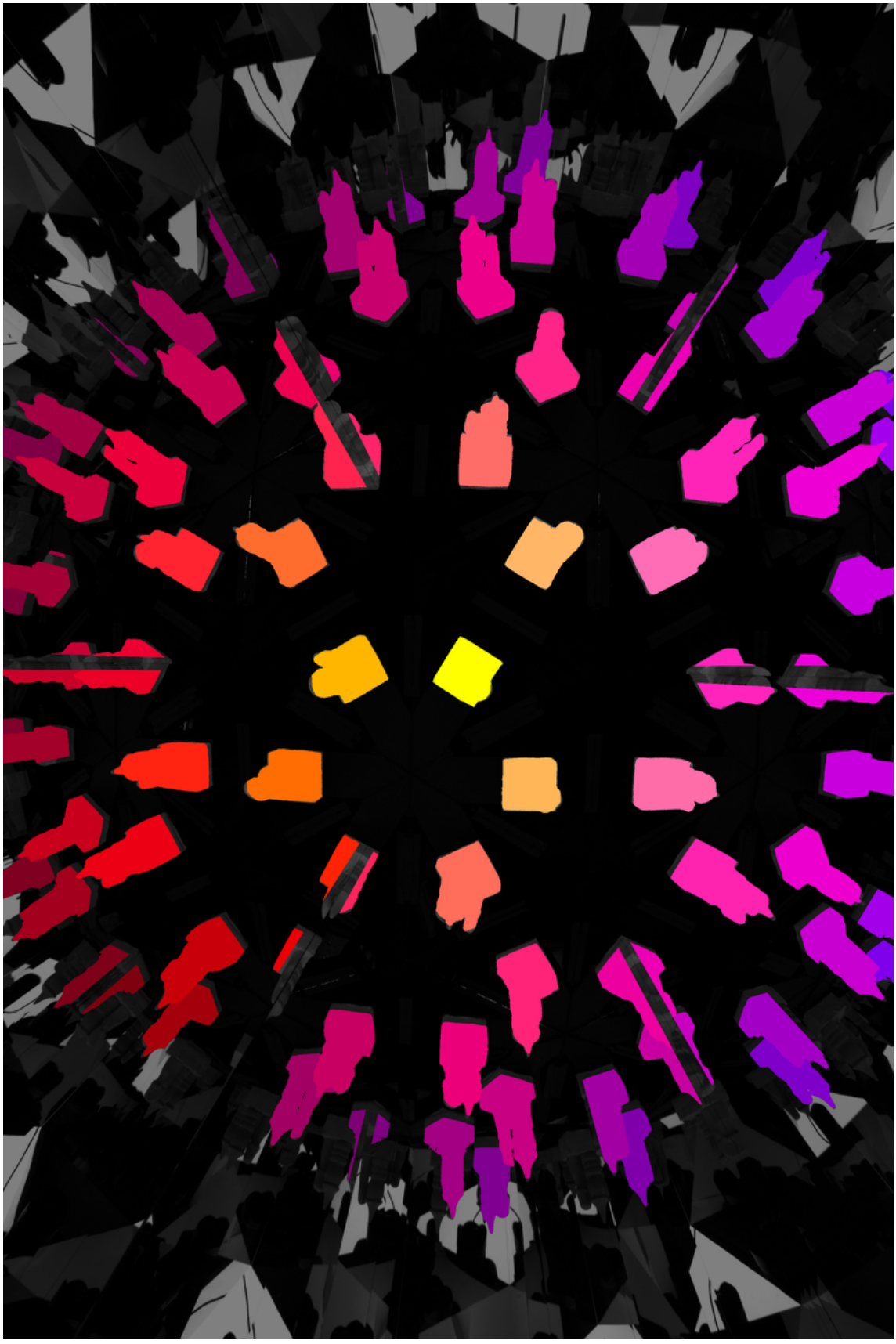

Figure 33. Chess data set - labeled image (7 reflection levels, 9 sub-samples per pixel)

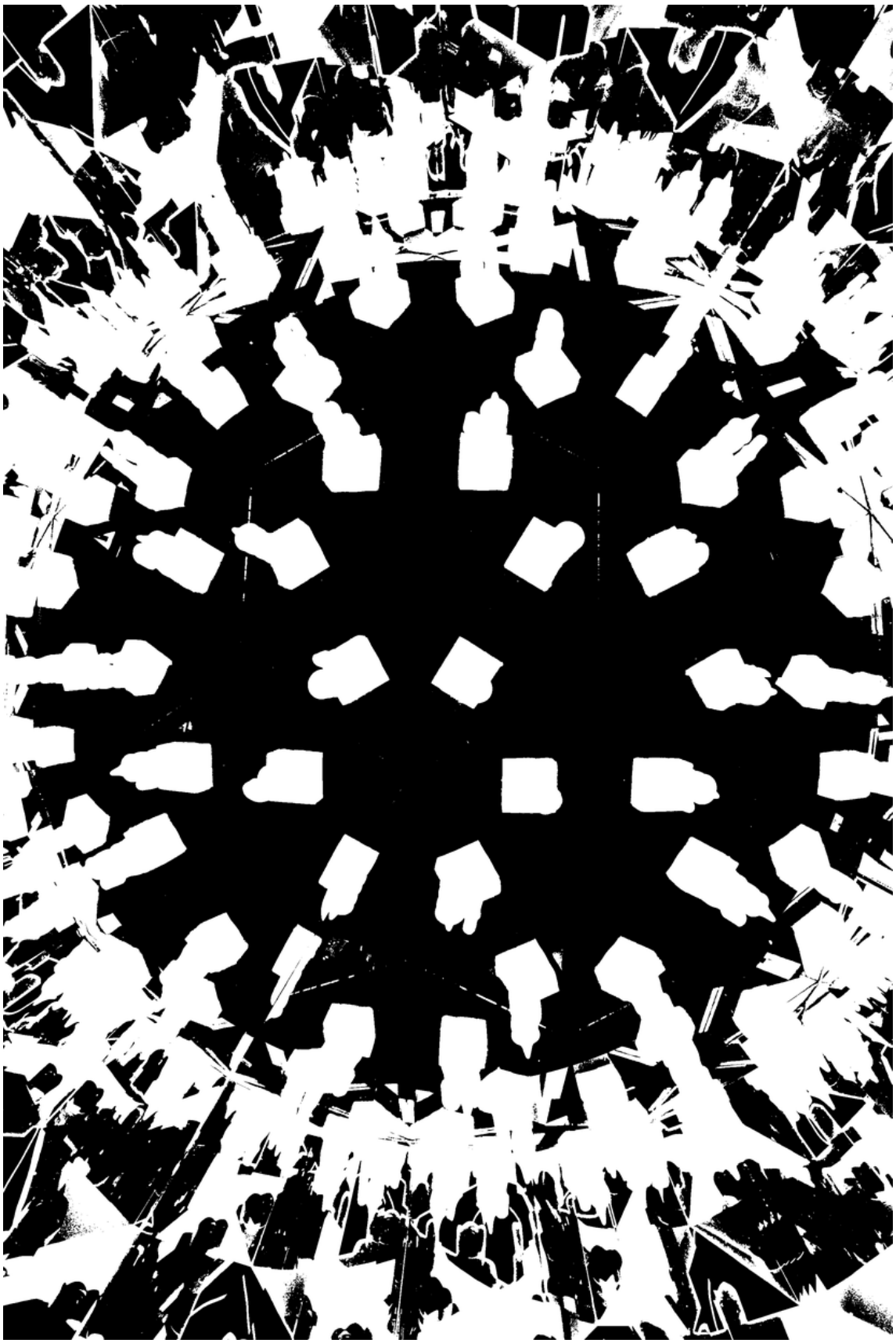

Figure 34. Chess data set - silhouette image used to compute labeling

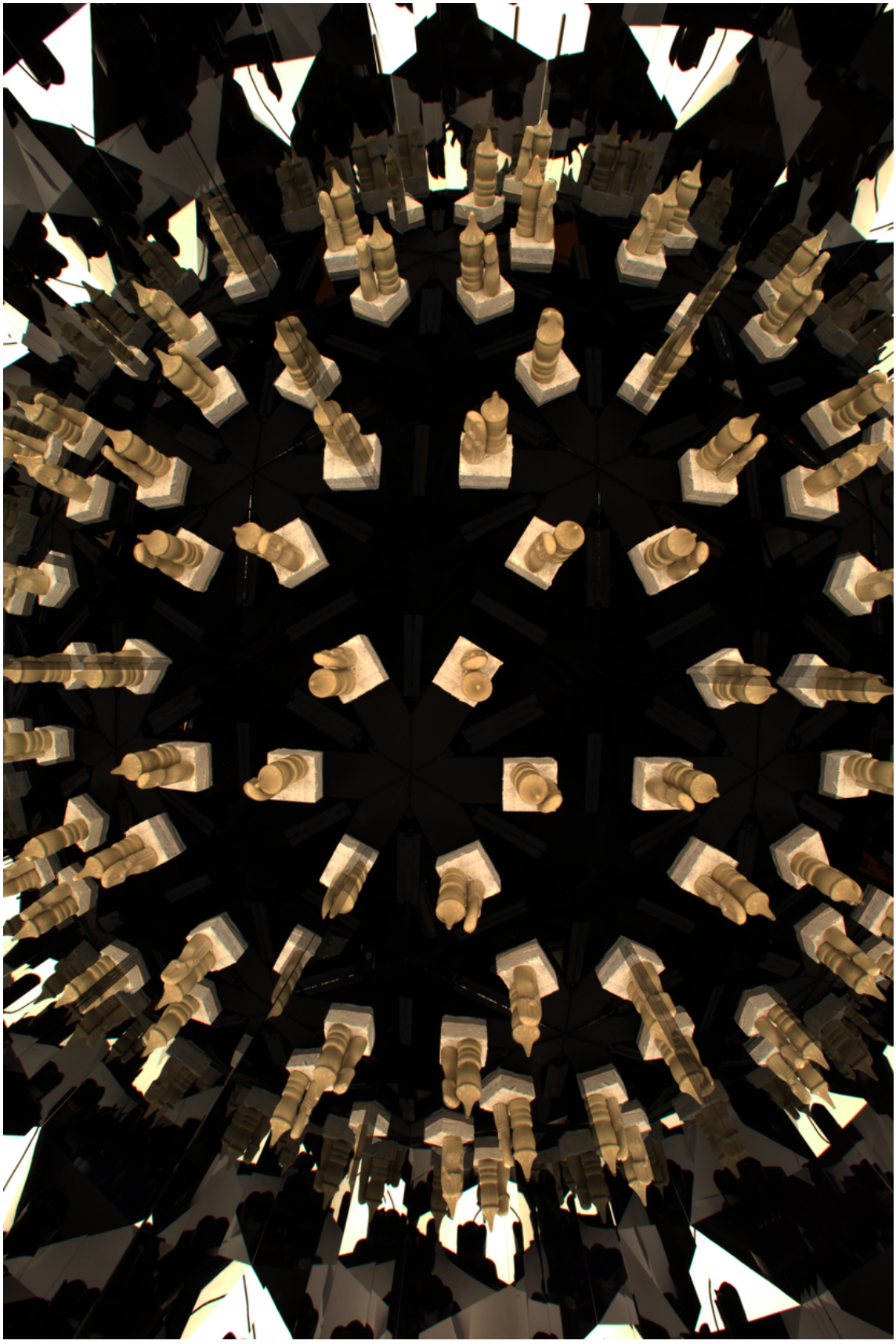

Figure 35. Chess data set - radiometrically compensated imaged

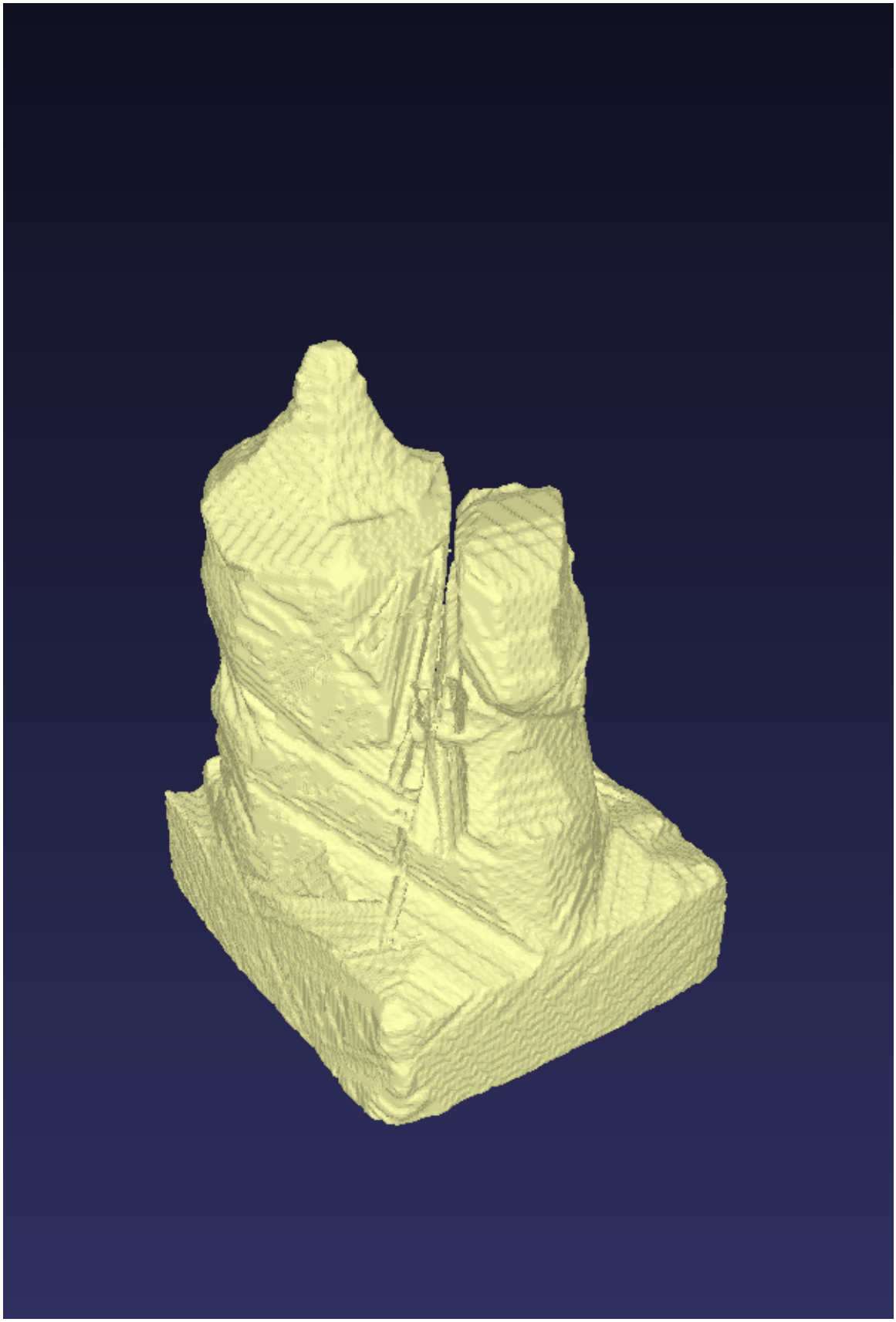

Figure 36. Chess data set - visual hull $256 \times 256 \times 354$

References

[1] A.Katok and B. Hasselblatt. Introduction to the Modern Theory of Dynamical Systems. 1997. 1